RAINFALL MORPHOLOGY IN SEMI-TROPICAL CONVERGENCE ZONES

Authors:

Lead Author and Correspondence Author:
Dr. J. Marshall Shepherd
NASA Goddard Space Flight Center
Laboratory for Atmospheres
Greenbelt, Maryland 20876

Second Author:
Dr. Brad S. Ferrier
Joint Center for Earth Systems
Technology/University of Maryland
Baltimore County
Baltimore, Maryland

Third Author:
Dr. Peter S. Ray
Florida State University
Department of Meteorology
Tallahassee, Florida 32306

RAINFALL MORPHOLOGY IN SEMI-TROPICAL CONVERGENCE ZONES

Abstract

Central Florida is the ideal test laboratory for studying convergence zone-induced convection. The region regularly experiences sea breeze fronts and rainfall-induced outflow boundaries. The focus of this study is the common yet poorly-studied convergence zone established by the interaction of the sea breeze front and an outflow boundary. Previous studies have investigated mechanisms primarily affecting storm initiation by such convergence zones. Few have focused on rainfall morphology yet these storms contribute a significant amount precipitation to the annual rainfall budget. Low-level convergence and mid-tropospheric moisture have both been shown to correlate with rainfall amounts in Florida. Using 2D and 3D numerical simulations, the roles of low-level convergence and mid-tropospheric moisture in rainfall evolution are examined.

The results indicate that time-averaged, vertical moisture flux (VMF) at the sea breeze front/outflow convergence zone is directly and linearly proportional to initial condensation rates. This proportionality establishes a similar relationship between VMF and initial rainfall. Vertical moisture flux, which encompasses depth and magnitude of convergence, is better correlated to initial rainfall production than surface moisture convergence. This extends early observational studies which linked rainfall in Florida to *surface* moisture convergence. The amount and distribution of mid-tropospheric moisture determines how rainfall associated with secondary cells develop. Rainfall amount and efficiency varied significantly over an observable range of relative humidities in the 850-500 mb layer even though rainfall evolution was similar during the initial or "first-cell" period. Rainfall variability was attributed to drier mid-tropospheric environments inhibiting secondary cell development through entrainment effects. Observationally, 850-500 mb moisture structure exhibits wider variability than lower level moisture, which is virtually always present in Florida. A likely consequence of the variability in 850-500 moisture is a stronger statistical correlation to rainfall, which observational studies have noted.

The study indicates that vertical moisture flux forcing at convergence zones is critical in determining rainfall in the initial stage of development but plays a *decreasing* role in rainfall evolution as the system matures. The mid-tropospheric moisture (e.g. environment) plays an *increasing* role in rainfall evolution as the system matures. This suggests the need to improve measurements of magnitude/depth of convergence and mid-tropospheric moisture distribution. It also highlights the need for better parameterization of entrainment and vertical moisture distribution in larger-scale models.

7.0 Introduction

Central Florida has the highest annual number of days with thunderstorms in the United States (Williams et al. 1992). Because of its unique geographical and meteorological conditions, Florida regularly experiences sea breeze fronts (SBF) and rainfall-induced, outflow boundaries (OB). The convergence associated with these phenomena or interactions between them can provide lift to initiate convection. Lines of single-cell and multi-cell thunderstorms with heavy rainfall and frequent lightning that last 1-2 h are common. Numerous observational and modeling studies have addressed aspects of convective development in Florida (Byers and Rodebush 1948; Day 1953; Gentry and Moore 1954; Frank et al. 1967; Pielke 1974; Ulanski and Garstang 1978a; Burpee 1979; Simpson et al. 1980; Tripoli and Cotton 1980; Cooper et al. 1982; Holle and Watson 1983; Nicholls et al. 1991; Arrit 1993; Halverson et al 1996; Fankhauser et al. 1995; Kingsmill 1995; Wilson and Megenhardt 1997).

Blanchard and Lopez (1985) identified three primary types of wind flows in the Florida summertime regime. Type I days are characterized primarily by an easterly component that causes the east coast SBF to propagate inland while the west coast SBF remains stationary. Type II days are characterized by an even stronger easterly component. Type III days are characterized by a westerly component that results in the greatest amount of convective activity in eastern Florida. This is primarily due to the east coast SBF remaining essentially stationary, while the west coast front and outflow boundaries interact with it. Figure 1 is a time history of visible GOES imagery over central Florida on 27 July 1991 and is an example of a Type III day. Convergence zone-induced lines of convection are prevalent in summertime Florida regardless of the prevailing wind flow.

Prior studies have focused mainly on the synoptic and meso-beta scale (50-200 km) organization of convection forced by convergence zones and, to a lesser extent, the storm/meso-gamma scale (1-50 km) organization. Although most of these studies have investigated factors primarily affecting storm initiation, few have focused on rainfall evolution in Florida storms. Any broad understanding of rainfall in Florida should consider small convective systems since they can contribute up to forty

percent of Florida's total annual rainfall. The National Aeronautics and Space Administration's (NASA) Tropical Rainfall Measuring Mission (TRMM) has established an extensive ground validation (GV) effort to understand tropical rainfall and its impact on global climate (Simpson et al., 1996). Central Florida is a primary GV site such that a study investigating rainfall morphology in Florida is timely.

Previous studies suggest that rainfall in Florida systems may be linked to surface convergence or mid-tropospheric moisture. Byers and Rodebush (1948), Ulanski and Garstang (1978a), and Tripoli and Cotton (1980) suggested that the amount of rainfall in Florida storms is correlated with areal extent and magnitude of *surface* convergence. However, recent findings suggest that surface convergence, though a necessary condition, is not sufficient to accurately correlate with rainfall production. Kingsmill (1995) examined a case in which an outflow boundary collided with a sea breeze front during the Convective and Precipitation Electrification Experiment (CaPE). He found no significant convective initiation or enhancement although favorable conditions (e.g., sufficient moisture, surface convergence, instability) were present. He theorized that there was sufficient convergence but the depth over which it was occurring was not sufficient to force parcels to their LFC. Wakimoto and Kingsmill (1995) found a similar occurrence. Such recent findings are consistent with earlier studies. Moore (1982) argued that an integrated moisture convergence parameter accounting for depth was more useful than a surface-based moisture convergence parameter for delineating severe storm and heavy rain events. Crook (1996) provided evidence in his simulations of a convergence zone system that an integrated moisture convergence parameter may have been more effective at identifying rainfall evolution. Xin and Reuter (1996) found that the amount of rainfall in a convective system was sensitive to amount and depth of convergence.

Other investigators have correlated rainfall in Florida with mid-tropospheric moisture (e.g., 850-500 mb). Frank and Smith (1968) found that the strongest correlation between percentage of radar echo and meteorological parameters was mid-tropospheric moisture, specifically 700-500 mb. Burpee (1979) found that variations in surface convergence could not explain the large differences in daily-averaged rainfall, but mid-tropospheric moisture could. Lopez et al. (1984) and Watson and

Blanchard (1984) provided evidence that "wet" days were more correlated with mid-tropospheric moisture. Burpee (1988) illustrated that on a rare summer day in Florida, there was virtually no convective rainfall throughout the entire peninsula due to an unusually dry middle troposphere. Watson et al. (1991) correlated 700-500 mb moisture with increased occurrences of lightning-producing storms. Fuelberg and Biggar (1994) found the largest variability, roughly 20%, in relative humidity for convective-nonconvective days was in the 700-500 mb layer.

This study seeks to provide a framework to couple low-level convergence and mid-tropospheric moisture to explain how they produce the most efficient rainfall system in the Florida convergence zone environment. A cloud-mesoscale model is employed to evaluate the sensitivity of rainfall morphology (e.g. lifecycle, amount, and efficiency) to magnitude of convergence, depth of convergence, and 850-500 mb moisture structure. This research contributes to and extends the current base of understanding of Florida convection in the following ways:

- The individual and synergistic roles of convergence magnitude, convergence depth, and mid-tropospheric moisture distribution are quantified in relation to rainfall morphology not just convective initiation at a convergence zone.
- 2D and 3D numerical simulations at storm (convective) scale provide new information on precipitation efficiency and rainfall production in Florida convection.
- The relative roles of vertical moisture flux and entrainment effects on rainfall development at a convergence zone are quantified.

The manuscript discusses the hypotheses of the study in section 2.0. Section 3.0 describes the numerical cloud/mesoscale model used in the experiments. Section 4.0 discusses the research methodology employed. Results of the 2D and 3D sensitivity experiments, trajectory analysis and conceptualizations are presented in section 5.0. Section 6.0 provides a summary and concluding remarks. Appendix A is the derivation of vertical moisture flux at a convergence zone.

2. Hypothesized factors affecting rainfall production in Florida convergence zone convection.

Byers and Braham (1949), Browning et al. (1976), Kingsmill and Wakimoto (1991), and Fovell and Tan (1998) have indicated that small convective thunderstorms (~1 hour life cycle) consist of one or more individual convective cells. Figure 2 is the descriptive model of Browning et al. (1976) illustrating the stages of development in a multicellular system. In figure 2, the following cells can be

identified: (1) *n-2*, oldest cell, (2) *n-1*, mature but decaying cell, (3) *n*, maturing cell formed at gust front produced by n-1 rainfall, and (4) *n+1*, early cell. Weisman and Klemp (1986) found that the ratio of buoyant energy and vertical wind shear, Bulk Richardson Number, is a good indicator of the likelihood of multicell thunderstorms. In Florida, the Bulk Richardson Number often falls into the category favorable for multicellular development (Wilson and Megenhardt 1997).

It is hypothesized that rainfall produced by the initial convective cell is directly proportional to area-averaged vertical moisture flux (VMF) (McIlveen 1986; Xin and Reuter 1996) at the convergence zone over a given time period prior to rainfall onset. VMF (in units of kg $m^{-2} s^{-1}$) at the convergence zone can be represented as:

$$VMF \cong \overline{\rho q M_{CZ}} Z_{CZ} \tag{1}$$

In equation 1, q is mixing ratio, ρ is a density term, M_{CZ} is convergence magnitude over the specified depth, and Z_{CZ} is convergence depth. Since density, mixing ratio and convergence magnitude vary with height, vertical averages over the depth Z_{CZ} are considered in the convergence zone region. Equation 1 indicates that *VMF* is altered by changes in the amount of moisture in the converging depth, the actual amount of convergence, or the depth of the convergence. Appendix A describes the derivation of vertical moisture flux (VMF). The hypothesis is based on the theory that early condensation rates should be directly proportional to the upward vertical moisture flux. This suggests a direct relationship between first-cell rainfall and VMF through the condensation rate-VMF proportionality. Another way to consider this theory is that in the initial stages of convective rainfall, there is virtually an instantaneous conversion of cloud water to precipitation because the condensation rate is proportional to the updraft (Rogers and Yau 1989; Doswell et al. 1996). For larger scales (> meso-gamma), longer time scales (> 30 min) after initial condensation, and under stronger shear conditions; these conditions may not hold.

It is further hypothesized that the amount and distribution of moisture in the middle troposphere (defined here as 850-500 mb) regulates the decay of the initial cell and the evolution of secondary cells. Rainfall produced by secondary cells is the primary contributor to total rainfall accumulation once the system transitions from the initial vertical moisture flux forcing in the first

cell. We propose that a dry mid-troposphere accelerates the decay of the initial cell and inhibits secondary cell development because of enhanced entrainment effects. The 850-500 mb layer is theorized to be an important source region for entraining air that affects secondary cell development. The possible effects of dry-air entrainment on tropical convective clouds has been investigated for many years (e.g. Simpson 1983). The basic idea is that dry environmental air is entrained into the cloud and mixed with rising air parcels, leading to dilution of parcel buoyancy. (Stommel 1947). However, Lucas (1998) remarked on the difficulties quantifying entrainment amount and source regions. To mitigate such difficulties, the effects of dry entrainment, defined as reduced cloud development (via condensation) and greater evaporation rates, are examined in this study. We suggest that growth of the first cell is linked to the vertical moisture flux forcing, while secondary cell growth and post-initial cell rainfall is primarily affected by environmental moisture. in the mid-troposphere.

3. Model

The numerical model employed in this study is the Center for Analysis and Prediction of Storms (CAPS) Regional Prediction System, ARPS, version 4.0. The ARPS model (CAPS, 1995) is a modular system that contains many physical and numerical options and is capable of 1-D, 2-D, or 3-D simulations. ARPS can resolve atmospheric systems on scales ranging from a few meters to hundreds of kilometers. Such flexibility makes simulations of smaller scale phenomena like thunderstorms, outflow boundaries, and sea breeze fronts possible. These phenomena are often parameterized or omitted in larger scale models.

The model is a non-hydrostatic atmospheric prediction model based on the compressible Navier-Stokes equations describing atmospheric flow. The system of equations to be integrated contains nine prognostic equations which include three momentum equations, the pressure and thermodynamic equations, moisture equations for various types of condensate, and a sub-grid kinetic energy equation. Table 1 describes key model parameters used in the model. A more complete discussion or model parameters and configurations is found in Shepherd (1999).

a. Two-dimensional model configuration

Recently, Kingsmill (1995) and Fankhauser et al. (1995) documented the three dimensional structure of the SBF/OB convergence zone environment. They found very sharp gradients in temperature, moisture, and wind. These gradients existed on scales ranging from a few hundred meters to 1.0 kilometer. These observational studies provide the basis for the model experiment configuration.

The model grid size is 80 x 17 km in the two-dimensional experiments (2D). The grid interval is 500 m in the horizontal and vertical direction. Sensitivity tests executed with vertical resolutions of 250 m and 500 m below 1.75 km were run to evaluate performance. Figure 3 illustrates slight differences in the evolution of maximum vertical velocity but generally, the system evolution in both sensitivity experiments is quite similar. It is equally encouraging that the magnitude of the velocities are consistent with vertical velocities observed in recent studies of Florida convection (e.g., Yuter and Houze 1995; Sun and Crook 1998). Such results provide confidence in our decision to use 500 m vertical resolution in the rainfall sensitivity experiments.

The model was integrated for 1.5 hours in time to capture the collision of the SBF and OB, initial formation of rainfall, maturation of the system, and decay of the system. The thermodynamic profile used for initialization is *based* on the 15 August 1991, 1956 UTC Deerpark CaPE sounding (figure 4a). On this day, active convection associated with a SBF/OB interaction was known to occur (Yuter and Houze 1995). However, the moisture profile was altered such that the mean relative humidity for the **CONTROL** run is 60 percent in the 850-500 mb layer. A mean of 60 percent was chosen based on Fuelberg and Biggar's (1994) study which found that mid-tropospheric moisture in Florida was generally near 60% but could vary by as much as 40%. Adjusting the 850-500 mb moisture to 60 percent facilitated easier comparisons with experiments in which moisture was altered in the layer.

The initial SBF (Simpson,1987) and OB (Charba 1974) were modeled as density currents approaching from the eastern and western portions of the domain, respectively. The density currents were inserted as linear profiles of potential temperature perturbation and wind speed, decreasing with height as in Mueller et al. (1993) and Crook (1991). They were inserted at opposite ends of the

domain. The depth, kinematic conditions, and thermodynamic compositions were based on Kingsmill (1995) and Fankauser et al. (1995). Kingsmill (1995) used CLASS soundings placed within a SBF and OB. He found that the OB reached depths of 1.7 km. The SBF was ~ 0.7 km. Kingsmill (1995) and Fankhauser et al. (1995) found using detailed PAM mesonet data and low-flying aircraft data that the ambient temperature deficit behind the SBF ranged from 1°-3° C while the ambient temperature deficit behind the OB ranged from 2°-10° C. In general, the sea breeze front air was roughly 1.0-2.0 g kg^{-1} moister than the intermediate or OB air.

For the outflow boundary, the leading edge of the density current was prescribed roughly 20 km from the western lateral boundary. It had a mean perturbation potential profile that decreased from ~-8.0 K to zero at 1.7 km. Crook (1991) and Mueller et al. (1993) noted that this type of profile is closer to the real vertical structure of outflow boundaries. Additionally, Chen (1995) found that the model performed better with linear profiles, especially near the top of the cold pool. He found that specifying a uniform temperature perturbation created spurious circulations near the top of the cold pool. The resulting outflow boundary (density current) propagated eastward with a mean potential temperature deficit of –4.0 K.

A similar configuration was used to model the sea breeze front except the leading edge of the density current was placed 40 km from the eastern boundary. In addition, the mean potential temperature deficit was only –1.5 K (decreasing from –3.0 K at the surface to 0.0 K near 0.7 km). Figure 5 is the initial 2D configuration of the perturbation potential temperature associated with the theoretical OB and SBF at t=15 minutes of simulation time in the **CONTROL** run. The SBF is the more shallow density current with surface easterly flow on the right side of the domain. The outflow boundary is the deeper density current with westerly flow on the left side of the domain. The SBF and OB collide at t≅15 minutes at gridpoint x≅28 km for the 2D **CONTROL** run.

b. Three-dimensional model configuration

In the 3D framework, the domain size was 60 km x 60 km x 17 km. The horizontal resolution was 1.0 km. This resolution is coarser than the 500 m resolution used in the 2D experiments. The 1.0 km resolution was still ample to resolve the major convective feature, yet not as computationally

expensive. Weisman et al.(1997) suggested that horizontal resolutions less than 4 km can explicitly resolve convective systems.

The SBF density current extended the entire length of the meridional axis. The OB density current was initialized as a 100 km^2 disk of cold air that extends to roughly 2.0 km in height. The perturbation potential temperature profile decreased linearly such that the mean value in the disk was –4.0 K. This initialization technique is very similar to the mechanism used by Chen (1995) to initiate an outflow boundary. As with the 2D configuration, the thermodynamic characteristics of the SBF and OB were based on observations from Fankhauser et al. (1995) and Kingsmill (1995).

The vertical resolution in the 3D experiments remained the same as the 2D configuration. Figure 6a illustrates the configuration of the SBF and OB (at the surface) at t=10 minutes of model time for the 3D CONTROL experiment. At this time, the eastward propagating OB is evident as the circular ring of enhanced surface moisture convergence. The linear enhanced region of surface moisture convergence denotes the simulated sea breeze front. Figure 6b illustrates the perturbation potential temperature field (surface) at t=10 minutes. The outflow boundary can be identified as the region of low perturbation potential temperature and divergent wind flow. The sea breeze front air is characterized by the southeasterly wind flow.

To simplify the analysis, simulations (in 2D and 3D) of the Type 3 day discussed by Blanchard and Lopez (1985) are used. Type 3 days are convective days in peninsular Florida characterized by a southwesterly to westerly component of the wind. It is on these days that the west coast SBF and modified outflow boundaries propagate eastward and interact with the virtually stationary east coast SBF. Type 3 days typically exhibit higher radar reflectivity echo coverage. The general interaction between a SBF and OB should be consistent on other type days, but this is certainly an additional area for future study. Figure 4b is the modified sounding used in the 3D experiments.

4.0 Research Methodology

The research was set within the framework of the Florida CaPE environment *though the study investigates theoretical system development as opposed to specific case study days.* The focus was the very common yet poorly-understood convergence zone established by the sea breeze front (SBF)

interacting with an outflow boundary (OB). Both two and three dimensional model experiments were conducted. The two-dimensional experiments were designed so that the variability of the parameter in question was within the dynamic range of variability observed near typical sea breeze front/outflow boundary convergence zones from the Florida Area Cumulus Experiment (FACE) and CaPE (Kingsmill 1995). Two sets of 2D experiments were conducted to ascertain the sensitivity of the rainfall evolution to: (1) convergence magnitude and depth and (2) mid-tropospheric moisture distribution. Each of the sensitivity experiments was compared to a **CONTROL** experiment based on the soundings in figure 4. The three-dimensional experiments were investigated as a sanity check on the two-dimensional work and was not meant to be exhaustive.

a. Integrated convergence experiments (2D)

The integrated convergence experiments were designed to ascertain whether initial rainfall is directly related to a parameter defined as the vertical moisture flux at 1.5 km. In other words, the initial moisture profile was assumed constant, and the investigation focused on how increasing vertical moisture flux (VMF) through changes in depth or magnitude affected rainfall development. Two experiments were included to elucidate the relative significance of convergence depth versus surface convergence magnitude.

The magnitude experiments were designed such that the changes in surface layer wind were within typical variability at a SBF or OB (Lee et al. 1991, Fankhauser et al. 1995). The depth experiments were also designed based on previous studies. The variability of the SBF depth (+/-500 m) is based on reports of the sea breeze front being relatively shallow (~200 m) as in Rao et al. (1998) to being relatively deep (~1200 m). The variability of the OB depth (-500 m) is based on studies such as Droegemeier and Wilhelmson (1985a), Lee et al. (1991), Kingsmill (1995) in which outflow boundary depth varied from a few hundred meters to 1700 meters. It was unrealistic to simulate a case in which outflow boundary depth was increased by 500 m. The main goal was to create variability in convergence depth and magnitude that is within reasonable dynamic range of observations. Table 2 describes the Integrated Convergence experiments.

b. Mid-tropospheric moisture experiments (2D)

The mid-tropospheric (850-500 mb) moisture experiments were designed to investigate how amount and distribution of moisture affect the precipitation efficiency and rainfall production. These experiments tested observational findings that mid-tropospheric moisture exhibits the strongest correlation to rainfall in Florida. Figure 7 illustrates the soundings as modified for each sensitivity experiment. Table 3 describes the Mid-Tropospheric Moisture experiments. Air parcel trajectories were computed, using the technique of Tao et al. (1995). The trajectory analyses were used to supplement findings in the Mid-Tropospheric Moisture experiments in terms of entrainment effects.

c. Three-dimensional experiments

Many of the convective lines that form along convergence zones appear to be quasi-two dimensional so that processes involved in rainfall production should reasonably be simulated with 2D model simulations. However, Nicholls et al. (1991) acknowledged that 3D work is needed at smaller scales to understand rainfall processes in Florida. Furthermore, recent work by Yuter and Houze (1995) suggested that Florida storms exhibit a great degree of three-dimensionality in terms of updraft-downdraft structure, microphysics, and rainfall. The objective was to test results from the 2D experiments in a 3D framework. This is a useful method of establishing robustness of conclusions drawn from the 2D results. However, the 3D work was not intended to be exhaustive and is another area where this work will be extended. Table 4 describes the 3D experiments.

d. Analysis parameters

The 2D and 3D results are investigated with respect to various parameters. The parameters are described in the following section:

i. Structure and Evolution

The evolution and morphology of the convective rainfall systems were investigated qualitatively using model calculated vertical velocity, mixing ratio perturbations, Convective Available Potential Energy (CAPE), and equivalent potential temperature. The primary low-level convergence parameters investigated were area/time-averaged, mean vertical moisture flux (<VMF>) at 1.5 km and area/time-averaged surface moisture convergence (<SMC>) at the SBF/OB convergence zone.

<VMF> and <SMC> were calculated from t=15 minutes to t=25 minutes of model run time as mean values over a 10 km area centered on the approximate collision point of the SBF and OB. Experience from test model runs suggested that a 10.0 km region was sufficient to resolve the low-level convergence at the SBF/OB collision point and its minimal movement within the initial 30 minutes.

ii. Quantitative Precipitation Amounts

The *total accumulated rainfall* (expressed kg km^{-1}) was defined as the total amount of rainfall in the model domain over the time integration of the model. The *first-cell accumulated rainfall* (expressed in kg km^{-1}) was defined as the amount of rainfall that accumulates from the beginning of the model run to a specific time after the relative minimum (roughly 40 minutes in this study) in condensation rate following the initial peak in that rate, as shown in figure 8. This parameter is arbitrarily defined to give some measure of first cell although some first cell contributions are likely to be present after 40 minutes. The *total surface area* was defined as the total surface area covered by at least 4.0 mm of rainfall at the end of 90 minutes (3D experiments only).

iii. Water Budgets

The budget of condensed water integrated over space and time in the full model domain is:

$$C = E + R + S, \tag{2}$$

where C is total condensation plus deposition of all ice species, E is total evaporation plus sublimation of ice, R is the total rainfall at the surface, and S is the mass of suspended condensate. *Precipitation efficiency (PE)* was calculated similar to Ferrier et al. (1996).

$$PE = R / C. \tag{3}$$

The microphysics package was structured such that time series and profiles of *condensation* and *evaporation* can be analyzed. It was also useful to analyze time series and profiles of *net condensation (NC)*

$$NC = C - E \tag{4}$$

Water budget constituents and rainfall amounts are only considered for a portion of the domain which encompasses the parent convective storm. This sub-domain resolves initial and secondary cell development but excludes spurious growth of cumulus clouds significantly distant from the parent

storm. These small cumulus clouds are related to outflow features downstream and near the lateral boundaries and do not produce rainfall. The parent storm is relatively stationary in relation to the initial sea breeze front/outflow boundary convergence zone. The sub-domain is centered at the collision point and is 20 km wide in order to resolve downstream secondary cells of the parent system. Figure 9 diagrams the sub-domain used in the study and illustrates cells within the domain and spurious convection (.e.g., at the downstream outflow boundary) outside of the analysis domain. Lessons from several experimental runs provide assurance that the multicellular activity of the parent storm is captured within the domain for this study.

5. Results

a. Two-dimensional integrated convergence experiments

Table 5 summarizes characteristics of the initial convection associated with the nine Integrated Convergence experiments. The table lists the time-averaged, mean surface moisture convergence (<SMC>), the area/time-averaged, mean vertical moisture flux (<VMF>) over lowest 1.5 km, and the amount of Convective Available Potential Energy (CAPE) at the initialization time. Table 5 also includes total domain accumulated surface rainfall and total condensation from the first convective cell (section 4.0). Generally, the experiments with larger <VMF> relative to **CONTROL** were associated with increased convergence magnitude at the surface (**CONV1.5**, **CONV1.5SBF-500**) or increased depth of convergence (**SBF500**, **OB-500**, **OB-500SBF500**). Likewise, experiments with smaller <VMF> were associated with reduced convergence magnitude at the surface (**CONV-1.5**, **CONV-1.5SBF500**) or reduced convergence depth (**SBF-500**).

In terms of initial rainfall produced by the first cell, total rainfall accumulations range from 1.9×10^8 kg km^{-1} to 3.4×10^8 kg km^{-1}. This result indicates that sensitivity experiments produce increases in initial rainfall as large as 30 percent and decreases as small as 27 percent compared to **CONTROL**. Tables 5 also indicates that experiments with large values of <VMF> generally produce more rainfall in the first cell relative to **CONTROL**. Similarly, experiments with small values of <VMF> produce less rainfall than **CONTROL**

A linear regression analysis was conducted to investigate the correlations between <VMF>, <SMC>, and total condensation and accumulated rainfall associated with the first convective cell. In the top panel of the figure 10, <VMF> is shown to be correlated (r=0.88) to the total condensation of the first cell. The middle panel illustrates a strong correlation (r=0.96) between <VMF> and the initial rainfall accumulation. The bottom panel indicates that <SMC> exhibits a weaker correlation (r=0.80) to initial rainfall accumulation. The weaker correlation between <SMC> and initial rainfall is primarily due to experiments **CONV-1.5SBF500** and **CONV1.5SBF-500**. These experiments are examples of how inverse changes in depth and magnitude can offset each other. An increase (decrease) in surface magnitude may be offset by a decrease (an increase) in convergence depth such that <VMF> might remain essentially constant. A good example of depth-magnitude offset can be observed with **CONV-1.5** and **CONV-1.5SBF500**. Both experiments possessed the same alteration of initial surface winds yet the <VMF> for **CONV-1.5** is 16% less than **CONV-1.5SBF500** which is compensated by deeper sea breeze convergence. *The stronger correlations for <VMF> are a direct result of the parameter encompassing convergence magnitude and depth. This extends early studies like Ulanski and Garstang (1978a) and Tripoli and Cotton (1980) that linked Florida rainfall to surface convergence features.* This also explains why surface convergence may not be sufficient to explain forcing in the initial convective cell as in Kingsmill (1995). Figure 11 indicates a direct and linear relationship between <VMF> and initial rainfall.

Figure 10 illustrates another key finding. Vertical moisture flux may be strongly linked to the initial rainfall through the condensation rate. This means that stronger <VMF> forcing would increase the condensation rate of the first convective cell, which ultimately leads to enhanced rainfall rates. Stronger rainrates produce larger accumulations. The basic premise can be stated in the following manner:

$$VMF \propto \text{condensation rate}, C \propto \text{initial rainfall.}$$

Another way to understand this relationship is through an approximate form of Doswell (1996)'s equation to represent rainfall in flash flood events. He stated that total rainfall amount, P, was related

to the vertical moisture flux, precipitation efficiency, and duration of rainfall. The approximation of the theorem used in this study takes the form:

$$P \cong RR \bullet dt, \tag{5}$$

$$\text{where } RR \cong \langle VMF \rangle \bullet PE^*$$

where RR is rainfall rate (mm hr^{-1}), PE^* is a truncated precipitation efficiency for the first cell, and dt is a specific time period. Figure 11 (bottom panel) illustrates that rainrates tend to peak near t=30 minutes, yet PE^* is fairly small at this time (~3-5 %). These facts suggests that RR is primarily a function of <VMF> in the early stages of development. The rainrate is computed as the mean of all gridpoints with measurable rain at each time. Figure 11 also plots the time series of sub-domain averaged condensation rate during the first 30 minutes of model run time for each 2D Integrated Convergence experiment.

The condensation rate in the upper panel illustrates that experiments with larger <VMF> produce instantaneous condensation rates which are 10-30% larger than **CONTROL**. Experiments with smaller <VMF> produce 10-30% smaller instantaneous condensation rates. The experiments with larger <VMF> also peak in condensation rate sooner than smaller <VMF> experiments, in some cases by as much as 3 to 5 minutes. The combined effect of more rapid and larger condensation rates explains why the rainrates at t=30 minutes are larger for experiments with larger <VMF>. The figure also illustrates an apparent lag of roughly 8-10 minutes between peak condensation rates (near 1300 s) and the peak rainrates (near 1800 s). It is observed that the relative minimum in condensation rate following the peak condensation rate coincides with the period of maximum rainfall intensity. This finding indicates that condensation processes in the first convective cell peak on the order of 10 minutes prior to the most intense rainrates. This is consistent with a study of radar first echoes in Florida by Hondl and Eilts (1994). They found that the time between first cell development (dBZ > 10) and dBZ values greater than 40 ranged from 5 to 45 minutes with the median time being 14 minutes.

In terms of the physical processes, larger values of vertical moisture flux at a convergence zone transport more moist static energy to the lifted condensation level. The availability of additional

moisture accelerates the condensation rate. The accelerated condensation rates produce more cloud water to be collected in the rainfall production process. As raindrops grow at the expense of the excess cloud water, rainrates increase in proportion to the increased <VMF> forcing and condensation rates. This explains the why mean domain rainrate in **CONV-1.5** is roughly 23% less than **CONTROL**, while the rate for **SBF500** is roughly 24% greater at t=1800 s.

b. Two-dimensional mid-tropospheric moisture experiments

The second component of our hypothesis argues that secondary cells, which develop in response to downdraft forcing from the initial cell, are regulated by the 850-500 mb moisture content. *The results suggest that the forcing-regulation relationship between vertical moisture flux and mid-tropospheric moisture may explain why a storm with similar convergent forcing may produce different rainfall totals on a given day.* To test the second component of our hypothesis, two sets of mid-tropospheric moisture experiments were conducted. One set of experiments investigated the sensitivity of rainfall evolution to bulk moisture changes in the 850-500 mb layer. Another set of experiments investigated the sensitivity of rainfall evolution to the distribution of moisture in the 850-500 mb layer.

i. Bulk moisture experiments

First, the results from the bulk moisture experiments are examined. Table 6 describes some of the initial characteristics of the Bulk Moisture experiments. It includes the name of the experiment, the mean precipitable water of the 850-500 mb layer, and CAPE of the pre-storm environment. The table illustrates that there is slight variability in the CAPE for each experiment. Primarily due to the introduction of variation of moisture, which slightly alters the virtual temperature profile used in the CAPE calculations. It is doubtful that the small changes in CAPE account for the larger variations in total rainfall and precipitation efficiencies in table 7.

Table 7 lists total condensation/deposition, total evaporation/sublimation, total surface rainfall, total suspendend condensate, and precipitation efficiency. In table 7, results indicate that a dry (moist) 850-500 mb layer produced a convective system that precipitated less (more) total rainfall and was less (more) efficient. **MID20** accumulated 42% less rainfall than **CONTROL**, while **MID80**

produced almost twice as much surface rainfall as **CONTROL**. In terms of PE, **MID80** was 10% more efficient than **CONTROL**, while **MID20** was 14% less efficient. This result supports Burpee's (1988) deduction that a rare, "no-rain" day in Florida was the result of a dry (~25 % RH) mid-troposphere. It is useful to recall that **CONTROL** has a mean relative humidity of 60%.

In general, the variability of PE ranges from 23% to 47% over the bulk moisture experiment parameter space. Braham (1952), using cloud data, found precipitation efficiencies in Florida storms to be near 19%. Ulanski and Garstang (1978a) found precipitation efficiencies in small storms to range from 37-54%. Neither investigator calculated PE values using total condensation and total surface rainfall as this study does. They calculated PE using estimates of moisture inflow at cloud base or the surface.

Our hypothesis links variability in rainfall production to rainfall that is produced (or not produced) by secondary cellular development. If this is true, rainfall evolution in the initial cell period should be similar for each experiment. Figure 12 plots the time evolution of precipitation efficiency (PE) in the bulk moisture experiments. In each experiment, the initial rainfall, inferred from PE evolution, evolves in roughly the same manner. This is concluded by noting that the time series coincide until roughly t=2000 s. After this time, PE deviates as a function of the 850-500 mb moisture profile in the experiments. *This deviation indicates that rainfall production after the initial VMF forcing of the first cell is a function of the mid-tropospheric moisture.*

Figure 13 plots vertical velocity and wind field flow at t=2100s for **CONTROL**, **MID20**, and **MID80**. This time is representative of the time period that secondary cell evolves in the system. In **MID20**, a weaker cell (local centroid of vertical velocity) centered near x=32.0 km and z=3.0 km has developed. A more vigorous cell developed in **MID80**. The cell in **MID20** is likely surpressed by increased entrainment effects due to the dry mid-tropospheric environment. We now investigates so-called "entrainment effects" to determine how they affect secondary cell development in the experiments.

The net condensation over the model time period is

$$NC(t) = C(t)-E(t), \tag{6}$$

where E(t) is the evaporation rate at a given time and C(t) is the condensation rate at a given time. The net condensation essentially provides a mechanism to see whether condensation or evaporative processes are dominant at a given time in the sub-domain. A negative value of NC indicates that evaporative processes are larger. Total suspended condensate is the sum of all hydrometeors (e.g., cloud water, rainwater, ice species) above ground level.

Figure 14 illustrates that during the earliest stages of development, the net condensation rate exhibits an inverse relationship to the amount of mid-level moisture. In other words, the drier experiments exhibit enhanced condensation in the first 5-15 minutes after the SBF/OB collision. However, the very important fact to observe is that the net condensation rates are similar between runs prior to 1500 s. Near t=2200 s, there is a secondary maximum in net condensation for **CONTROL**, **MID40**, and **MID80**. This maximum is associated with secondary cell development. The results suggest that condensation associated with the secondary cell for **MID80** is quite vigorous but virtually non-existent for **MID20**. This explains why values of condensation in table 7 are larger for **MID80**.

Lucas (1998) noted that entrainment could reduce mass flux in clouds by evaporating available liquid water in the cloud, cooling the parcel, and reducing buoyancy. This would lead to lower rates of condensation. Examining the time series of total suspended condensate, results indicate that more hydrometeor species are suspended following t=2200 s in **MID80**. Secondary cell development has proceeded with less effect from entrainment and evaporative processes. In the "drier" experiments, total suspended condensate exhibits a steady decay after an initial peak associated with the initial cell. Again, the suggestion is that drier mid-levels promote entrainment of dry air which evaporates water vapor in growing secondary convective cells and the initial mature cell. This limits the amount of suspended condensate (e.g. cloud water, ice, etc.) that can develop. Brown and Zhang (1997) observed similar results in their investigation of cloud top development in the warm pool region of the Pacific ocean.

To investigate entrainment effects further, an analysis of cloud layer evaporation profiles was performed. Figure 15 displays profiles of total evaporation from the LCL to 10.0 km in the sub-

domain of this study. Evaporative processes are larger below 500 mb in the "drier" experiments such as **MID20** and **MID40** and smaller in **MID80**. These results also indicate that the *effects* of entrainment are greater when the 850-500 mb layer is drier, which serves to inhibit secondary cell growth. This fact ultimately leads to reduced precipitation efficiency and rainfall accumulations in the total system.

ii. Moisture distribution experiments

Drier (moister) mid-levels hinders (enhances) the development of rainfall by increasing (reducing) the effects of entrainment in the saturated updrafts that support cell development. Lin and Arakawa (1997a,b) and Lucas (1998) recently investigated what role the vertical distribution of moisture plays. Both investigators found that moistening of the lowest levels up to 3.0 km was most critical. In Florida, observational studies (Frank and Smith 1968; Burpee 1979; Fuelberg and Biggar 1994) have consistently shown that mid-tropospheric moisture, specifically 700-500 mb, exhibit strong correlations to rainfall activity in Florida. The study investigates the role of the moisture distribution using a set of experiments in which the distribution of moisture is changed. Section 4.0 described the moisture distributions for each experiment.

Table 8 describes the experiments in terms of mean precipitable water and CAPE. CAPE values are fairly consistent for the dry and moist experiments, respectively. The mean initial precipitable water (mm) was calculated for the 850-500 mb layer for each of the distribution experiments. For all experiments in which water vapor was added (**MOIST850700, MOIST700500, MOISTPAR**), mean PW in the 850-500 mb layer was equal to 22.0, 22.4, and 21.8 mm, respectively. For all experiments in which water vapor was removed (**DRY850700, DRY700500, DRYPAR**), mean PW in the 850-500 mb layer was equal to 16.9, 15.1, and 14.9 mm, respectively. These results illustrate that though 700-500 mb layer is thicker. It also contains less water vapor such that increases in relative humidity in this layer will generally be offset by the moister lower region, and vice-versa. Since 850-500 mb water vapor is virtually conserved over the mid-tropospheric dry and moist distribution experiments, it is instructive to investigate how the actual distribution in the layer affects rainfall evolution and secondary cell development.

Table 9 lists results condensation, evaporation, total suspended condensate, rainfall amount, and precipitation efficiency. Examining the experiments, drying the 850-700 mb or 700-500 mb layer by similar magnitudes produces roughly the same amount of rainfall and similar precipitation efficiencies. However, the drier experiments generally produce 15% less rainfall and are less-efficient rainfall producers than **CONTROL**, while the moist experiments generally produce on the order of 35% more rainfall and are slightly more efficient.

In figure 16, as with the bulk moisture experiments, the initial rainfall evolution, depicted by the time series of precipitation efficiency, is quite similar in the distribution experiments. The experiments that are drier or moister in the 700-500 mb layer (e.g., **DRYPAR**, **MOISTPAR**, **DRY700500**, **MOIST700500**) exhibit the largest variability from **CONTROL** during secondary cell development after 2000 s.

Results in table 9 indicate that similar variations in moisture in the upper or lower portion of the 850-500 mb layer can produce similar rainfall totals. This means that moistening or drying the atmosphere from 3.0-5.5 km can affect rainfall in the same manner as moistening or drying levels below 3.0 km. This is different from Lin and Arakawa (1997a) and Lucas (1998) who found that moisture up to roughly 3.0 km was critical to explain variability in convection through moisture distribution changes. Both of these studies examined oceanic convection with low cloud bases, larger wind shear environments, and moving cloud systems. In such environments, upshear tilted systems may likely be affected more by lower level moisture. In the convergence zone systems of this study, there was weak wind shear and higher cloud bases. Additionally, the storms were virtually erect and possibly even downshear tilted. A westerly wind aloft also "blows through" the storm which is essentially stationary relative to the initial convergence point. Ferrier et al. (1996) found that erect storms in moist mid-level environments are more efficient at producing rainfall. Our findings along with Ferrier et al. (1996) indicate *that the typically erect storms of the Florida convergence zone environment may be significantly hindered by entrainment-effects from dry-midtroposheric air.*

Using the forward trajectory analysis of Tao et al. (1995), it is shown that air parcels penetrate the cloud region (1.5-10.0 km) from all levels. Forward trajectories were calculated for the **CONTROL**

experiment (figure 17) to illustrate that air parcels may enter the cloudy region of a growing cell from levels ranging from 850-500 mb. The parcels were released at various levels in the 850-500 mb layer east of the eventual cloud region at t=0 sec and followed for 1.5 hours. The figure illustrates that some parcels in the 850-700 mb layer are entrained into the updraft region and detrained at 7.0-9.0 km. Other parcels are transported downward. Parcels between 3.6-4.7 km are entrained into the updraft region but exit the cloud region near 3.0-3.3 km. This suggests that air above 700 mb can be transported downstream and to lower levels where secondary cell development is favored. Parcels in the upper layer of the 700-500 mb layer can also be entrained into the system's updraft and detrained near 9.0 km. The 700-500 mb layer can exert as much control over updraft and secondary cell evolution as the 850-700 layer.

Profiles of total evaporation in figure 18 illustrate that most of the variability in evaporation occurs below 6.0 km. Above this level, evaporation profiles are quite similar. The experiments which produce the largest increases in evaporation relative to **CONTROL** are **DRY700500** and **DRYPAR**. The net increases are as large as 30-50% and peak between 2200-3300 m. This indicates that dry environmental air above 3.0 km is likely entraining into regions below 3.0 km to promote evaporation of developing secondary cells. Similarly, the largest reductions in evaporation are observed in **MOIST700500** and **MOISTPAR**. This indicates that the effects of air entraining from the 700-500 mb are not as detrimental for secondary cell growth when the upper layer is moist. Observing the profiles of **MOIST850700** and **DRY850700**, they behave quite similarly to **CONTROL**. This would indicate that evaporative effects are more influential for a dry 700-500 mb layer. This finding is consistent with Frank and Smith (1968), Burpee (1988), Watson et al. (1991), and Fuelberg and Biggar (1994).

Moisture variability in the 850-700 mb and 700-500 mb layer can affect total rainfall production in convergence zone systems. This result indicates that for a given forcing, the low to middle tropospheric moisture up to 5.5 km can significantly impact rainfall evolution and efficiency. Since low-level moisture is virtually ubiquitous in Florida in the summer months, these results explain why mid-tropospheric moisture exhibits a strong statistical correlation to rainfall. *The mid-tropospheric*

moisture is likely to exhibit a wider range in variability, whereas moisture below 850 mb is virtually constant.

c. Three-dimensional experiments

Since the atmosphere is three-dimensional not two-dimensional, a subset of 3D runs were done to verify the 2D modeling results *though they were not meant to be exhaustive.* In the 3D experiments, the outflow boundary collides with the sea breeze front near t=15 minutes, and the first surface rainfall appears 15-25 minutes later. This is consistent with the 2D results. Table 10 and figure 19 show results consistent with the hypotheses and 2D results. The experiments that possess a deeper initial convergence zone (e.g. larger <VMF>) (**DRY700500+SBF 500**and **CONTROL+SBF500**) generally produce 2-2.5 times more initial rain than **CONTROL**.

Examining the respective systems towards the latter stages of their lifecycle, it can be inferred that vertical moisture flux plays a decreasing role as the system matures, while mid-tropospheric moisture plays an increasing role. Table 10 indicates that in terms of total rainfall, the experiments that possessed larger <VMF> at the convergence zone produced 11% *more* rainfall (**CONTROL+SBF500**) and 25% *less* rainfall (**DRY700500+SBF500**) than **CONTROL**, respectively. **DRY700500+SBF500** ultimately produces less total rainfall than **CONTROL** yet produces more rainfall in the initial stages. This result is an indication that total rainfall in small STCZ convective systems is strongly modulated by the ability of secondary cells to evolve. The general distribution of rainfall is similar for all experiments in figure 19, however, the **VERYDRY700500** experiment produced an area of rain roughly 50-65% less than all other experiments. The dry mid-tropospheric air reduces the magnitude and area of rainfall, contributing to a less-productive rainfall system.

d. Conceptualization of Rainfall Evolution in Convergence Zone Systems in Florida.

The goal now is to tie the results together into a coherent picture of the evolution of convective rainfall forced by a typical Florida convergence zone interaction (e.g. a SBF/OB collision). Figure 20 is the time series of total accumulated rainfall for the 3D experiments. At the earliest time periods, the 3D experiments with convergence over a deeper layer (e.g. larger <VMF>) produce the most

rainfall. However, as the system evolves, the influence of the initial convergent forcing lessens, and the regulatory effect of the mid-tropospheric moisture becomes more important. The trace for experiment **DRY700500+SBF500** is an excellent example of this transition process. Before 3000 s, **DRY700500+SBF500** produces more rainfall than the systems with more shallow convergence (e.g., smaller <VMF>), but after 3000 sec it is exceeded by the CONTROL run. Secondary cell growth is affected by entrainment in the 700-500 mb dry layer

Recently, Fovell and Tan (1998) presented a theoretical description of cell evolution in a multicell system. Fovell and Tan (1998) suggested that the buoyancy-induced circulations associated with developing cells may entrain environmental air. Dry air in the 850-500 layer could reduce the buoyancy-induced circulation as air is entrained from the sides and the top of the newly-generated cell. Evidence from this study confirms that secondary cell responds strongly to the environmental moisture in the 850-500 mb layer. The coupling of this study's findings and those of Fovell and Tan (1998) should be extended in future work.

Figure 21 is a schematic that illustrates the general findings of the study. Rainfall accumulation stage is along the ordinate, ranging from initial rainfall to total rainfall accumulation. It is essentially depiction of time evolution. The abcissa indicate the relative influence rating of vertical moisture flux forcing and mid-tropospheric moisture. *In the figure, it is suggested that vertical moisture flux forcing is the stronger influence on initial rainfall, associated primarily with the first convective cell. However, this influence decreases as secondary cells evolve. Environmental moisture in the mid-troposphere takes on a stronger influence as secondary cells evolve. The moisture regulates the decay of the initial cell once the initial burst of rainfall linked to VMF forcing subsides. More importantly, the moisture regulates how effectively secondary cells evolve.* Future work should investigate this theory under different synoptic patterns and wind shear regimes.

6.0 Summary and Conclusions

This study was unique in its attempt to couple low-level convergence (magnitude and depth) at a common Florida convergence zone with mid-tropospheric moisture to understand the relative and synergistic importance of each to rainfall production. More specifically, the purpose was to identify

and quantify how rainfall development (e.g., initial rainfall, total amount, precipitation efficiency) at a typical Florida convergence zone is influenced by the observationally significant low-level convergence and mid-tropospheric moisture fields. This research is different from many previous studies in that the focus was on rainfall morphology at convergence zones, not convective initiation.

a. Conclusions

The key findings of the study are summarized below:

- Initial rainfall morphology is related not only to the amount of low-level convergence but to the depth of the convergence. This extends early studies like Ulanski and Garstang (1978a) and Tripoli and Cotton (1980) which linked Florida rainfall to magnitude and areal extent of *surface* convergence only.

- There is a direct and linear relationship between time-averaged vertical moisture flux (which encompasses depth and magnitude) at a convergence zone and initial rainfall. Increasing (decreasing) time-averaged vertical moisture flux over an observable range of convergence zone conditions produces variability in initial rainfall on the order of +/-25%. Weaker correlations exist between time-averaged surface convergence and initial rainfall.

- Vertical moisture flux-initial rainfall relationship is established through the condensation rate. This can be stated simply in the following manner:

$$<VMF> \propto \text{condensation rate, } C \propto \text{initial rainfall.}$$

- For the observable range (+/- 20%)of variance in relative humidity in the mid-troposphere (850-500 mb), PE varied from 23% to 47% while total rainfall accumulation varied by almost a factor of two. The bulk changes in moisture produced relatively large variations in PE and total rainfall amount, but initial rainfall evolved in roughly the same manner. Rainfall from the initial cell responded to a given vertical moisture flux, but, the total rainfall was regulated by the ambient 850-500 mb moisture. The findings indicates that the regulation is directly related to how the 850-500 moisture content affects secondary convective cell development through entrainment effects (e.g., evaporation). Such results quantify, using models, what numerous investigators have observed in Florida systems.

- The dry mid-tropospheric experiments produced significantly weaker secondary convective cells, while the moist experiments produced vigorous secondary cell development. This fact was indicated by evidence of relatively high net condensation rates and suspended condensate after the initial cell in the "moist" experiments. Likewise, "drier" experiments produced larger reductions in net condensation and suspended condensate following the initial cell, which

indicated that secondary convective activity was being reduced by evaporation processes. The evidence indicates that drier (moister) mid-levels hinders (enhances) the development of rainfall by increasing (reducing) the effects of entrainment in the saturated updrafts.

- Drying or moistening the 850-700 mb or 700-500 mb layer by comparable amounts produced similar variations in rainfall production and efficiency. Moisture variability in the 3.0-5.5 km layer can affect rainfall as much as moisture variability at lower levels. This is different from Lin and Arakawa (1997a) and Lucas (1998) who found that moisture up to roughly 3.0 km was critical to explain variability in convection through moisture distribution changes. Both of those studies examined oceanic convection with low cloud bases, larger wind shear environments, and moving cloud systems. In such environments, upshear tilted systems may likely be affected more by lower level moisture. In the convergence zone systems of this study, there was weak wind shear and higher cloud bases. Additionally, the storms were virtually erect and possibly even downshear tilted. A westerly wind aloft also "blows through" the storm which is essentially stationary relative to the initial convergence point. All of these factors are theorized to play a role in allowing the mid-troposphere to exert significant influence on entrainment-related effects like cloud evaporation and condensation rates.

- Since low-level moisture is virtually ubiquitous in Florida in the summer months, study results explain why mid-tropospheric (700-500 mb) moisture exhibits a strong statistical correlation to rainfall. The mid-tropospheric moisture is likely to exhibit a wider range of variability, whereas lower level moisture is virtually constant. Still, the mid-troposhpheric moisture variability is critical to rainfall evolution.

- Three-dimensional experiments confirmed the basic findings of the two-dimensional experiments. Vertical moisture flux played a *decreasing* role rainfall formation as the system matured, while mid-tropospheric moisture played an *increasing* role. This was supported by results in which experiments with larger initial vertical moisture flux produced greater accumulations initially (e.g., first cell). Yet, total accumulations and areal extent of accumulations were a function of the 850-500 mb moisture.

b. Implications

This study unified two schools of observation (low-level convergence and mid-tropospheric moisture) concerning the production of rainfall in small, Florida convective systems typical during summer months. Additionally, the research provided a much needed assessment of the precipitation efficiency and rainfall potential of storms produced at common Florida convergence zones. This work also extended the body of 2D and 3D numerical modeling studies of Florida convection at

convective/meso-gamma scale. This study also highlighted the need for improved measurement of low-level convergence magnitude, convergence depth, and mid-tropospheric moisture. This suggests the need to be more attentive to efforts to parameterize the effects of entrainment in larger-scale models. Furthermore, the results suggest that the nature of the role of entrainment effects and ambient moisture in convection may differ for storms depending on several factors. Such factors include whether they are oceanic or land based systems, erect or tilted systems, or systems embedded in weak or strong shear environments. All of these areas are appropriate for future investigations.

Acknowledgements. This research was sponsored by the National Aeronautics and Space Administration through the NASA-Goddard Space Flight Center Research and Study Fellowship. The authors are grateful to B. Adler, F. Einaudi, V. Salomonson, and D. Menchan for their support. Thanks are also due to B. Lynn for the providing the satellite data and the ARPS Group at CAPS for providing the model and insight concerning its use.

Appendix A

Derivation of Vertical Moisture Flux at the Model Convergence Zones

For the purpose of this study, upward vertical moisture flux (2D) at a convergence zone (e.g. over the depth below the LCL) is derived from the anelastic continuity equation in the following manner:

Start from $$\frac{\partial q}{\partial t} = \frac{dq}{dt} - \frac{\partial}{\partial y}(uq) - \frac{\partial}{\partial y}(vq) - \frac{1}{\rho}\frac{\partial(\rho wq)}{\partial z}, \tag{1}$$

Rearranging terms yields,

$$\frac{1}{\rho}\frac{\partial(\rho wq)}{dz} = \frac{dq}{dt} - \frac{\partial q}{\partial t} - \frac{\partial(uq)}{\partial x} - \frac{\partial(vq)}{dy}$$

$$= \frac{dq}{dt} - \frac{\partial q}{\partial t} - q\left(\frac{\partial u}{\partial x} + \frac{\partial v}{\partial y}\right) - u\frac{\partial q}{\partial x} - v\frac{\partial q}{\partial y} \tag{2}$$

$$\frac{\partial(\rho wq)}{\partial z} = \rho\frac{dq}{dt} - \rho\frac{\partial q}{\partial t} - \rho q M^{*}_{CZ} - \rho u\frac{\partial q}{\partial x} - \rho v\frac{\partial q}{\partial y}, \tag{3}$$

where $$M^{*}_{CZ} = \frac{\partial u}{\partial x} + \frac{\partial v}{\partial y}.$$

Ignoring the first two terms on the right side and solving, neglecting meriodional gradients in (3),

$$\frac{\partial(\rho wq)}{\partial z} \cong -\rho q M^{*}_{CZ} - \rho u\frac{\partial q}{\partial x}, \tag{4}$$

Integrating (4) with height (where M_{CZ}=-M^{*}_{CZ}),

$$(\rho wq)_{Z_{CZ}} - (\rho wq)_0 \cong \int_0^{Z_{CZ}} \rho q M_{CZ}\, dz - \int_0^{Z_{CZ}} \rho u\frac{\partial q}{\partial x} dz, \tag{5}$$

Neglecting the last term on the right and simplifying terms yields,

$$VMF \cong (\rho wq)_{Z_{CZ}} \cong (\rho wq)_0 + \overline{\rho q M_{CZ}} Z_{CZ} \tag{6}$$

The justification for neglecting the advection term in equation 5 is based on two factors: First, only magnitude and depth of convergence are varied in the study while the low-level moisture gradient is constant in the experiments. Second, aircraft and surface observations from CaPE (see Fankhauser et al. 1995-figure 8) suggest that at the SBF/OB collision point, the gradient in moisture may approach zero over a sufficient distance since mixing ratio is often similar behind the OB and

SBF. Scaling analysis indicates that the first term on the right side of equation 5 is much larger than the second term.

The first and second terms on the left in equation 6 represent surface fluxes of moisture and fluxes of moisture due to integrated convergence, respectively. At the small time scales of this study (~ 1-90 minutes), the second term >> the first term. For example, the mean VMF and surface moisture flux were computed over 10.0 km centered at the SBF/OB collision point at t=15 minutes. The mean VMF and surface flux were approximately 42.4 kg $m^{-2}s^{-1}$ and 0.1 kg $m^{-2}s^{-1}$, respectively.

7.0 References

A National Science Foundation's Science and Technology Center for Analysis and Prediction of Storms' Advanced Regional Prediction System Documentation, 1995. K. Droegemeier, Director, 374 pp.

Arritt, R.W., 1993: Effects of the large-scale flow on characteristic features of the sea breeze. *J. Appl. Meteor.*, **32**, 116-125.

Blanchard, D.O. and R.E. Lopez, 1985: Spatial patterns of convection in south Florida. *Mon. Wea. Rev.*, **113**, 1282-1299.

Braham, R.R., 1952: The water and energy budgets of the thunderstorm and their relation to thunderstorm development. *J. Meteor.* **9**, 227-242.

Brown, R.G. and C. Zhang, 1997: Variability of midtropospheric moisture and its effects on cloud-top height distribution during TOGA COARE. *J. Atmos. Sci.*, **54**, 2760-2774.

Browning, K.A., J.C. Fankhauser, J.-P. Chalon, P.J. Eccles, R.C. Strauch, F.H. Merrem, D.J. Musil, E.L. May, and W. R. Sand, 196: Structure of an evolving hailstorm. Part V: Synthesis and implications for hail growth and hail suprression. *Mon. Wea. Rev.*, **104**, 603-610.

Burpee, R.W., 1979: Peninsula-scale convergence in the south Florida sea breeze. *Mon. Wea. Rev.*, **107**, 852-860.

Burpee, R.W., 1988: A summer day without significant rainfall in south Florida. *Mon. Wea. Rev.*, **1**, 680-687.

Byers, H.R., and R.R. Braham, Jr., 1949: *The Thunderstorm*. U.S. Govt. Printing Office, 287 pp.

Byers, H.R. and H.R. Rodebush, 1948: Causes of thunderstorms of the Florida peninsula. *J. Meteor.*, **5**, 275-280.

Charba, J., 1974: Application of gravity current model to analysis of a squall-line gust front. *Mon. Wea. Rev.*, **102**, 140-156.

Chen, C., 1995: Numerical simulations of gravity currents in uniform shear flows. *Mon. Wea. Rev.*, **11**, 3240-3253.

Cooper, H.J., M. Garstang, and J. Simpson, 1982: The diurnal interaction between convection and peninsular-scale forcing over South Florida. *Mon. Wea. Rev.*, **110**, 486-503.

Crook, N.A, 1991: Small-scale moisture variability in the convective boundary layer and its implications for nowcasting. Preprints, 25th Conference on Radar Meteorology., Paris, France, Amer. Meteor. Soc., 314-320.

Crook, N.A., 1996: Sensitivity of moist convection forced by boundary layer processes to low-level thermodynamic fields. *Mon. Wea. Rev.*, **124**, 1767-1785.

Day, S., 1953: Horizontal convergence and the occurrence of summer shower precipitation at Miami, Florida. *Mon. Wea. Rev.*, **81**, 155-161.

Doswell, C.A., H.E. Brooks, and R.A. Maddox, 1996: Flash flood forecasing: An ingredients-based methodology. *Wea. and Forecasting.* **11**, 560-581.

Droegemeier, K.K. and R.B. Wilhelmson, 1985a: Three-dimensional numerical modeling of convection produced by interacting thunderstorm outflows. Part I: Control simulation and low-level moisture variations. *J. Atmos. Sci.*, **42**, 2381-2403.

Fankhauser, J.C., N.A. Crook, J. Tuttle, L.J. Miller, and C.G. Wade, 1995: Initiation of deep convection along boundary layer convergence lines in a semitropical environment. *Mon. Wea. Rev.*, **123**, 291-313.

Ferrier, B.S., J. Simpson, and W.K. Tao, 1996: Factors responsible for precipitation efficiencies in midlatitude and tropical squall simulations. *Mon. Wea. Rev.*, **124**, 2100-2125.

Fovell, R.G., and P.H. Tan, 1998: The temporal behavior of numerically simulated multi-cell-type storms. Part II: The convective cell life cycle and cell regeneration. *Mon. Wea. Rev.*, **126**, 551-577.

Frank, N.L., P.L. Moore and G.E. Fisher, 1967: Summer shower distribution over the Florida peninsula as deduced from digitized radar data. *J. Appl. Meteor.*, **6**, 309- 316.

Frank, N.L., and D.L. Smith, 1968: On the correlation of radar echoes over Florida with various meteorological parameters. *J. Appl. Meteor.*, **7**, 712-714.

Fuelberg, H.E. and D. Biggar, 1994: The preconvective environment of summer thunderstorms over the Florida panhandle. *Weather and Forecasting*, **9**, 316-326.

Gentry, R.C., and P.L. Moore, 1954: Relation of local and general wind interaction near the sea coast to time and location of airmass showers. *J. Meteor.*, **11**, 507-511.

Halverson, J., M. Garstang, J. Scale, and W.-K. Tao, 1996: Water and energy budgets of a Florida Mesoscale convective system: A combined observational and modeling study. *Mon. Wea. Rev.*, **124**, 1161-1180.

Holle, R.L. and A.I. Watson, 1983: Duration of convective events related to visible cloud, convergence, radar and raingage parameters in south Florida. *Mon Wea. Rev.*, **111**, 1046-1051.

Hondl, K.D. and M.D. Eilts, 1994: Doppler radar signatures of developing thunderstorms and their potential to indicate the onset of cloud-to-ground lightning. *Mon. Wea. Rev.*, **122**, 1818-1836.

Kessler, E., 1969: On the distribution and continuity of water substance in atmospheric circulation. *Meteor. Monogr.*, **24**, No. 46, Amer. Meteor. Soc., 165-170.

Kingsmill, D., 1995: Convection initiation associated with a sea-breeze front, a gust front, and their collision. *Mon. Wea. Rev.*, **123**, 2913-2933.

Lee, B.D., R.D. Farley, and M.R. Hjelmelt, 1991: A numerical case study of convection initiation along colliding convergence boundaries in northeast Colorado. *J. Atmos. Sci.*, **48**, 2350-2366.

Lin, C., and A. Arakawa, 1997a: The macroscopic entrainment processes of simulated cumulus ensemble. Part I: Entrainment sources. *J. Atmos. Sci.*, **54**, 1027-1043.

Lin, C., and A. Arakawa, 1997b: The macroscopic entrainment processes of simulated cumulus ensemble. Part II: Testing the entraining plume model. *J. Atmos. Sci.*, **54**, 1044-1053.

Lopez, R.E., P.T. Gannon, D.O. Blanchard, and C.C. Balch, 1984: Synoptic and regional circulation parameters associated with the degree of convective shower activity in south Florida. *Mon. Wea. Rev.*, **112**, 686-703.

Lucas, C., 1998: Environmental variability during TOGA COARE and its effect on mesoscale convective systems: observations and modeling. Ph.D Dissertation. Texas A & M University, 175 pp.

McIlveen, J.F.R., 1986: *Basic Meteorology-A Physical Outline.* Van Nostrand Reinhold, 457 pp.

Moore, J.T., 1982: The forcing and evolution of the three dimensional moisture convergence during the 10-11 April 1979 severe weather outbreak. Preprints 12th Conf. Severe Local Storms, San Antonio, Amer. Meteor. Soc., 209-212.

Mueller, C.K., J.W. Wilson, and N.A. Crook, 1993: The utility of sounding and mesonet data to nowcast thunderstorm initiation. *Wea. Forecasting*, **8**, 132-146.

Nicholls, M.E., R.A. Pielke, and W.R. Cotton, 1991: A two-dimensional numerical investigation of the interaction between sea breezes and deep convection over the Florida peninsula. *Mon. Wea. Rev.*, **119**, 298-323.

Pielke, R., 1974: A three-dimensional model of the seabreeze over south Florida. *Mon. Wea. Rev.*, **102**, 115-139.

Rao, P. A., H. E. Fuelberg, and K. K. Droegemeier, 1999: High resolution modeling of the Cape Canaveral area land/water circulations and associated features. In press *Mon. Wea. Rev.*

Rogers, R.R., and M.K. Yau, 1989: *A Short Course in Cloud Physics.* Pergamon Press., New York, 293 pp.

Shepherd, J.M., 1999: Rainfall morphology in semi-tropical convergence zones. Ph.D Thesis, Florida State University, Tallahassee, 119 pp.

Simpson, J., N.E. Westcott, R.J. Clerman and R.A. Pielke, 1980: On cumulus mergers. *Arch. Meteor. Geophys. Bioklim.*, **A29**, 1-40.

Simpson, J., 1983: Cumulus clouds: Early aircraft observations and entrainment hypotheses. *Mesoscale Meteorology-Theories, Observations and Models*, D.K. Lilly and T. Gal-Chen, Eds., 355-373.

Simpson, J., C. Kummerow, W.-K. Tao, and R.F. Adler, 1996: On the Tropical Rainfall Measuring Mission (TRMM). *Meteorol. Atmos. Phys.*, **60**, 19-36.

Simpson, J.E., 1987: *Gravity Currents: In the Environment and the Laboratory.* John Wiley and Sons, 244 pp.

Stommel, H., 1947: Entrainment of air into a cumulus cloud. *J. Meteor.*, **4**, 91-94.

Sun, J. and N.A. Crook, 1998: Dynamical and microphysical retrieval from Doppler Radar observations using a cloud model and its adjoint. Part II: Retrieval experiments of an observed florida convective storm. *J. Atmos. Sci.*, **55**, 835-852.

Tao, W.K., J.R. Scala, B. Ferrier, and J. Simpson, 1995: The effect of melting processes on the development of a tropical and a midlatitude squall line. *J. Atmos. Sci.*, **52**, 1934-1948.

Tripoli, G.J., and W.R. Cotton, 1980: A numerical investigation of several factors contributing to the observed variable intensity of deep convection over south Florida. *J. Appl. Meteor.*, **19**, 1037-1063.

Ulanski S.L. and M. Garstang, 1978a: The role of surface divergence and vorticity in the life cycle of convective rainfall, Part I: Observation and analysis. *J. Atmos. Sci.*, **35**, 1047-1062.

Watson, A.I., and D.O. Blanchard, 1984: The relationship between total area divergence and convective precipitation in south Florida. *Mon. Wea. Rev.*, **112**, 673-685.

Watson, A.I., R.L. Holle, R.E. Lopez, R. Ortiz, and J.R. Nicholson, 1991: Surface wind convergence as a short term predictor of cloud-to-ground lightning at Kennedy Space Center. Wea. And Forecasting, 6, 49-64.

Weisman, M.L. and J.B. Klemp, 1986: Characteristics of isolated convective storms. *Mesoscale Meteorology and Forecasting*, P.S. Ray, Ed., Amer. Meteor. Soc., 331- 358.

Weisman, M.L., W.C. Skamarock, J.B. Klemp, 1997: The resolution dependence of explicitly model convective systems. *Mon. Wea. Rev.*, **125**, 527-548.

Williams, S., K. Caeser, and K. Southwick, 1992: Convection and Precipitation Experiment Operations Summary and Data Inventory. Office of Field Project Support. Boulder, 425 pp.

Wilson, J.W. and W.E. Schreiber, 1986: Initiation of convective storms by radar-observed boundary layer convergence lines. *Mon. Wea. Rev.*, **114**, 2516-2536.

Wilson, J.W. and D.L. Megenhardt, 1997: Thunderstorm initiation, organization, and lifetime associated with Florida boundary convergence lines. *Mon. Wea. Rev.*, **125**, 1507-1525.

Xin L. and G.W. Reuter, 1996: Numerical simulation of the effects of mesoscale convergence on convective rain showers. *Mon. Wea. Rev.*, **124**, 2828-2842.

Xu, H., 1997: Simulations of sea breeze induced convection using the ARPS model. M.S. Thesis, The Florida State University, pp. 96.

Yuter, S.E. and R.A. Houze, Jr., 1995: Three-Dimensional kinematic and microphysical evolution of florida cumulonimbus. Part I: Spatial distribution of updrafts, downdrafts, and precipitation. *Mon. Wea. Rev.*, **123**, 1921-1940

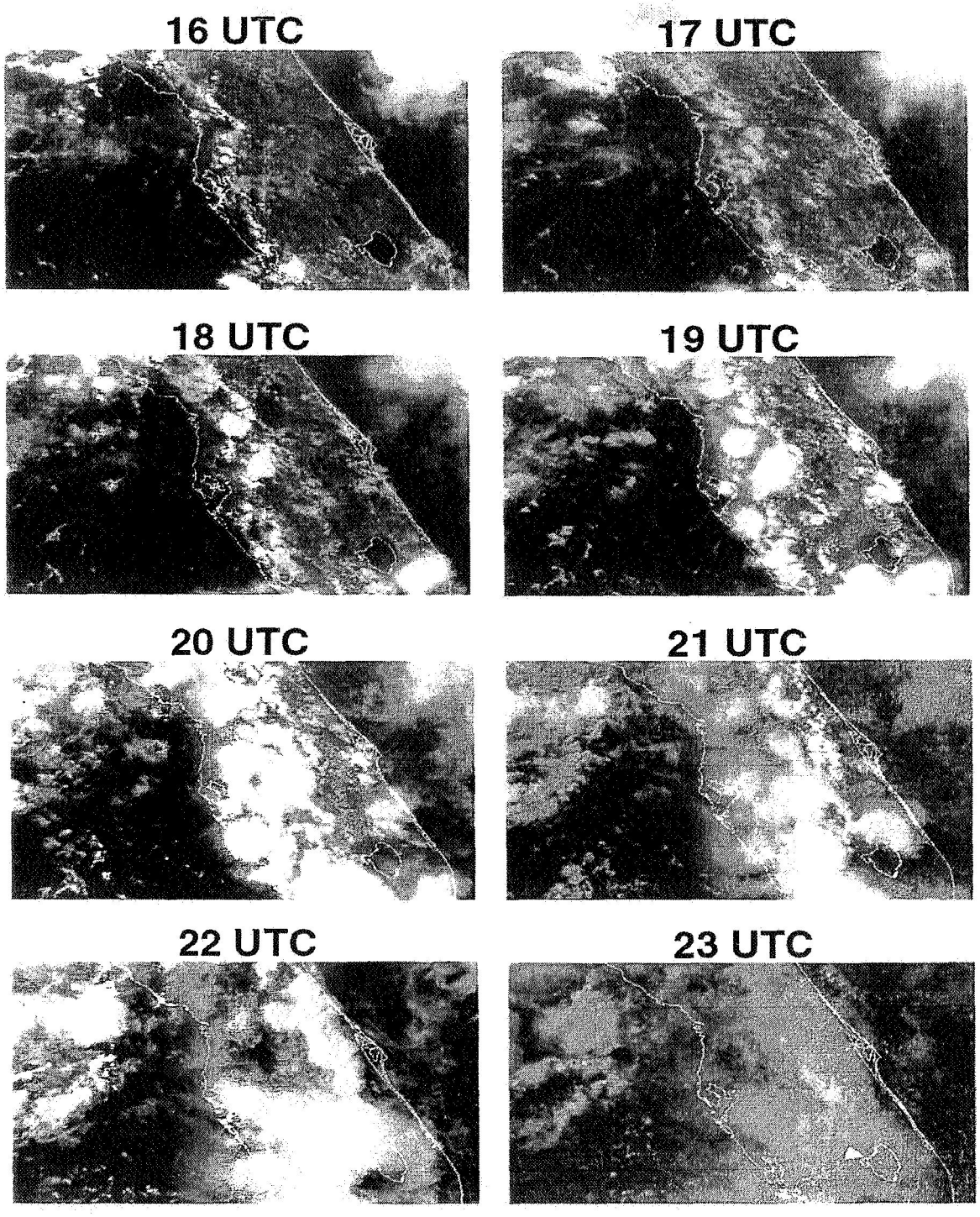

Figure 1-Time history of visible GOES satellite imagery on 27 July 1991 in central Florida.

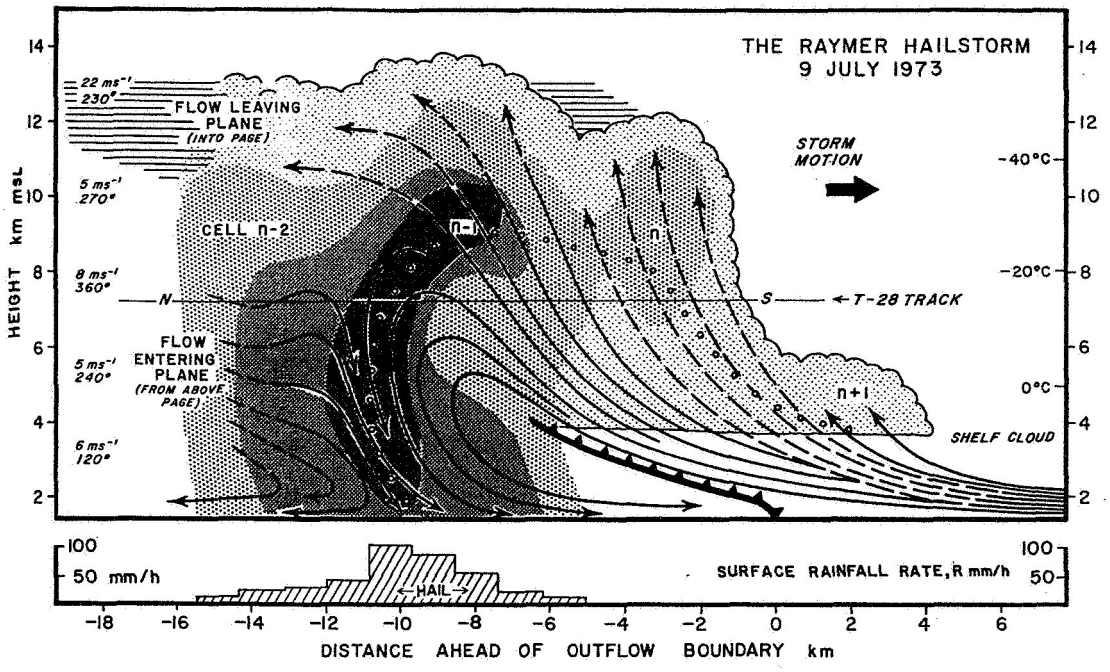

Figure 2-Descriptive model of a multicell thunderstorm (following Browning et al., 1976).

a.

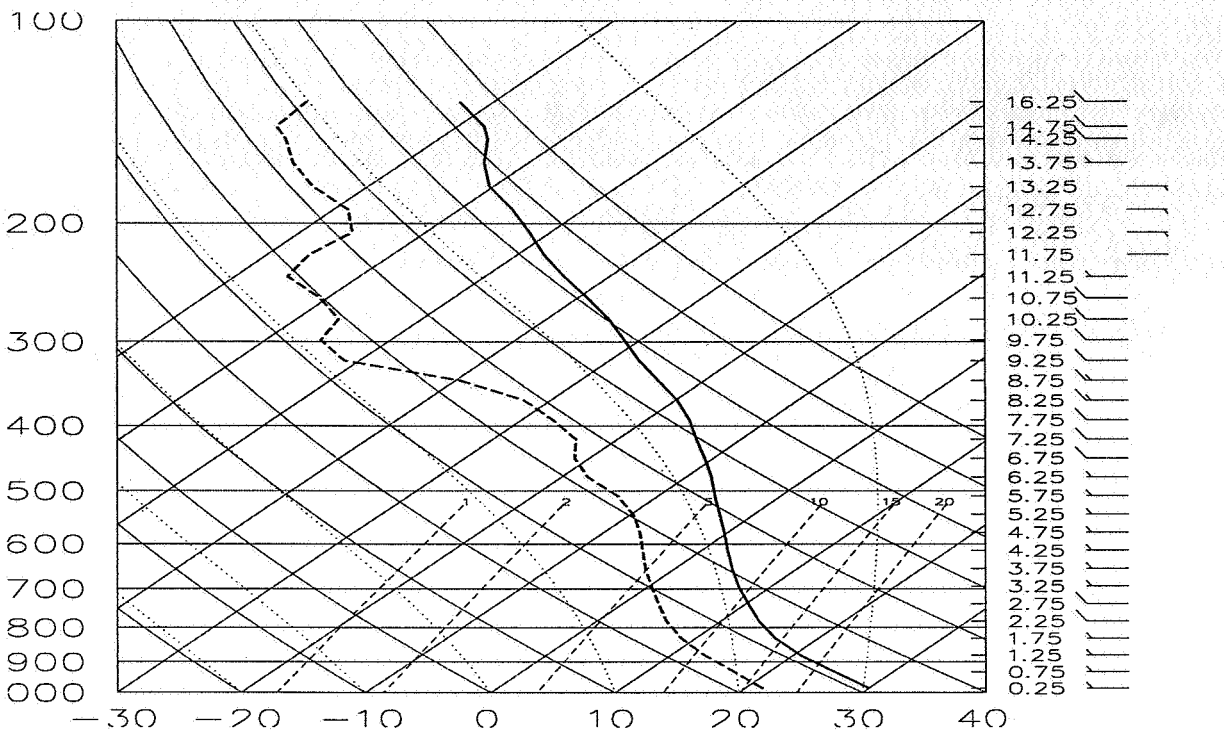

b.

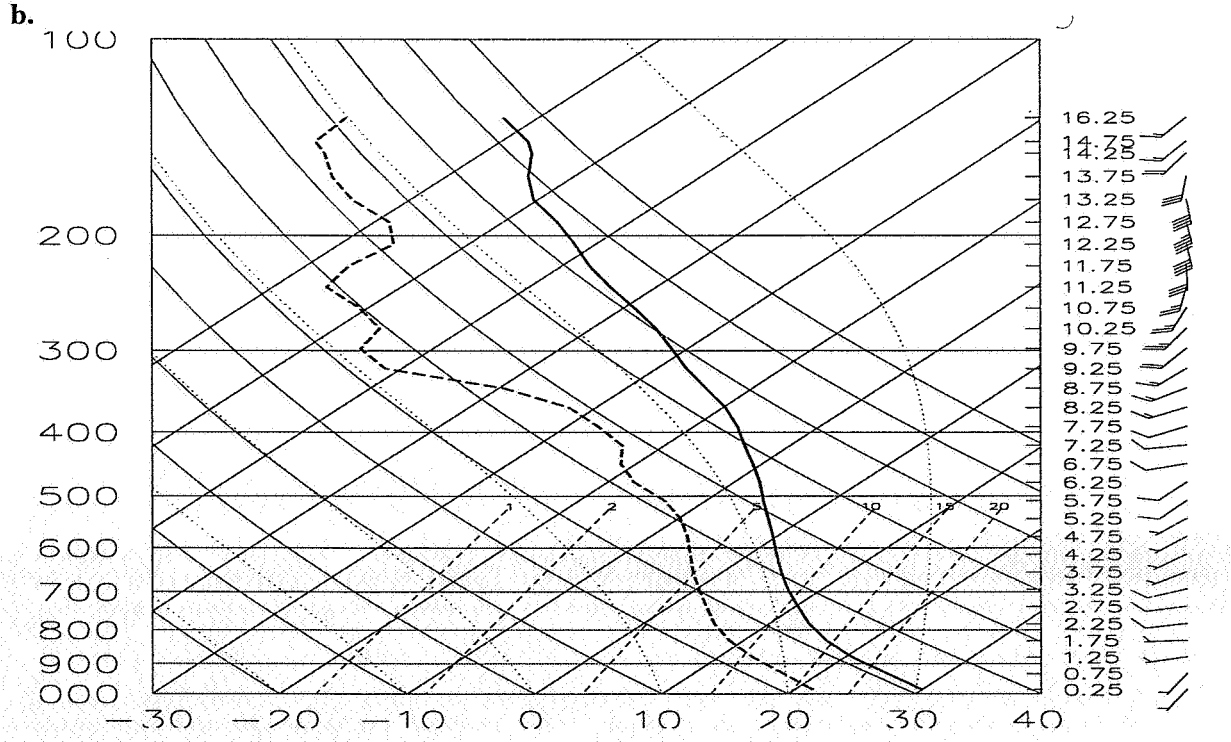

Figure 4-Modified 1956 UTC Deerpark Sounding for 15 August 1991 a. 2D experiments b. 3D experiments.

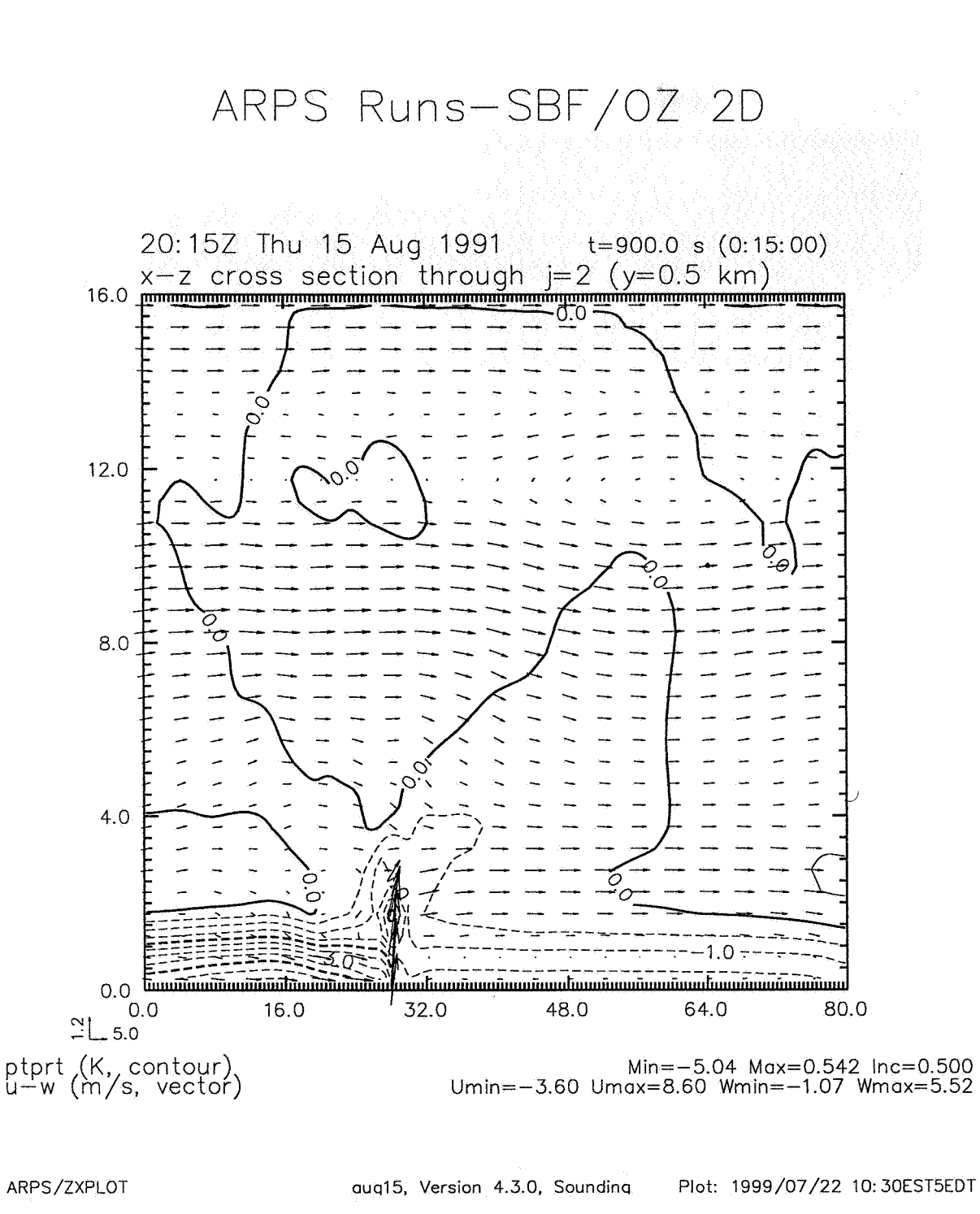

Figure 5-Configuration of SBF and OB at t=15 minutes in 2D control run. The plot is an overlay of perturbation potential temperature (K) and wind vectors (m s^{-1}).

a.

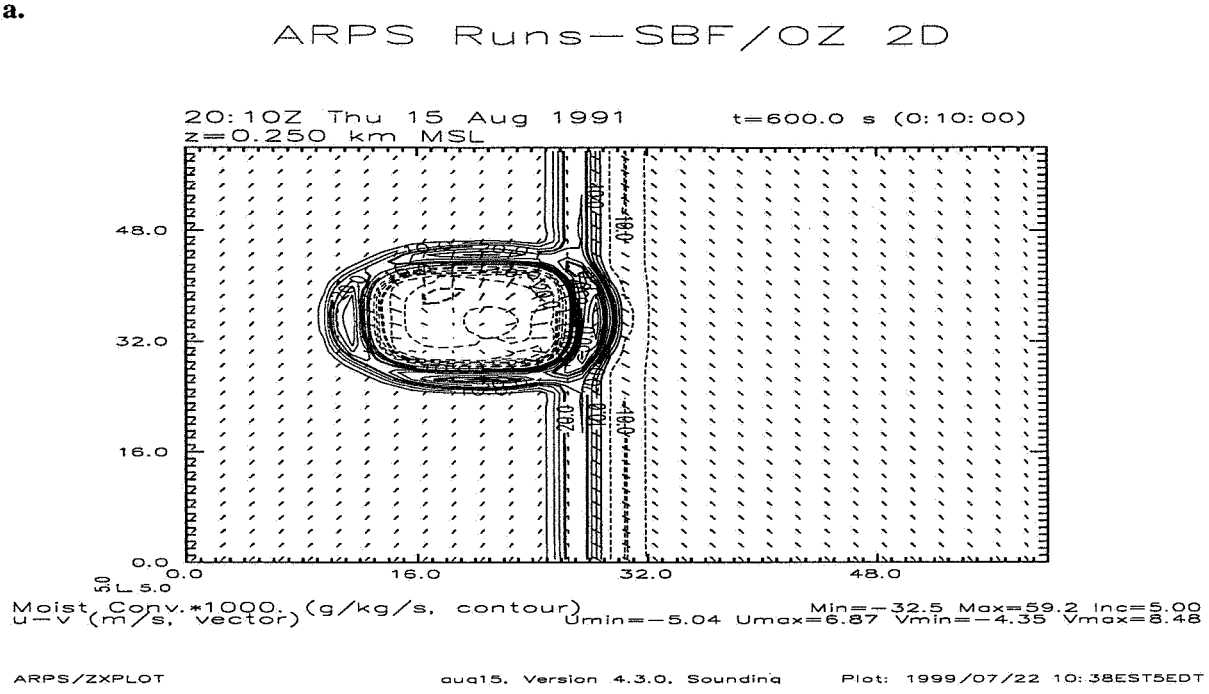

b.

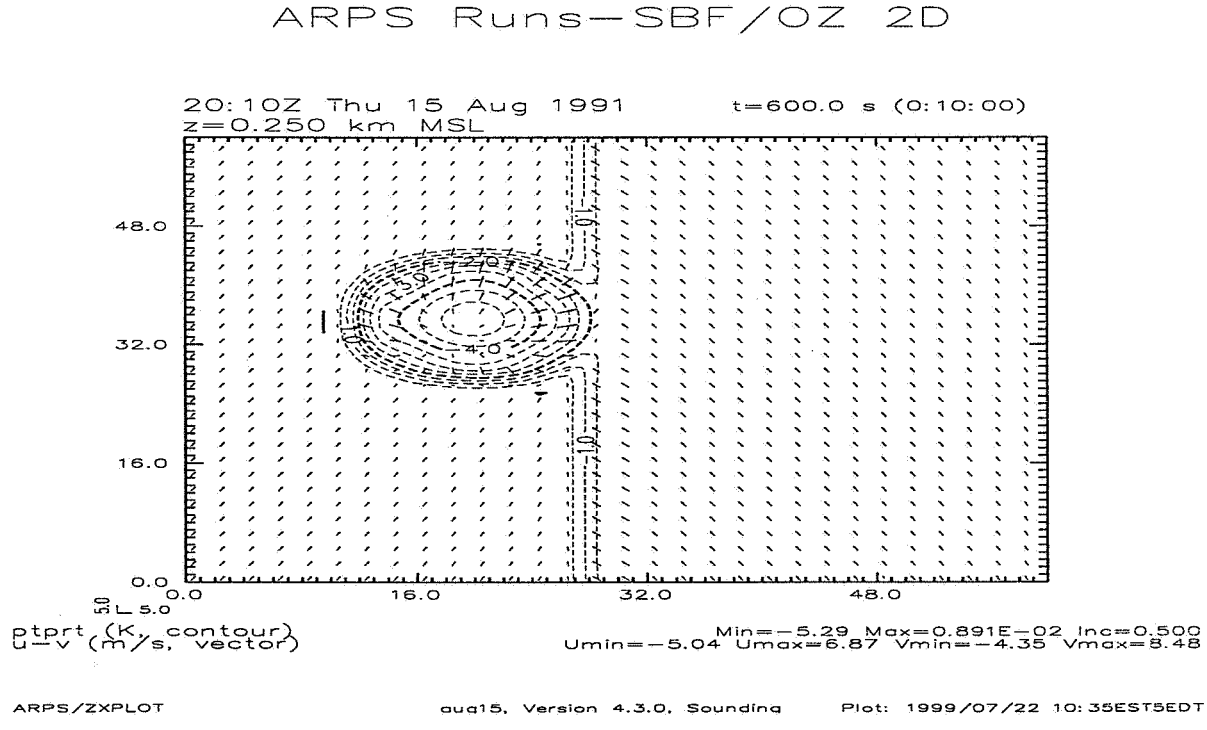

Figure 6-Configuration of SBF and OB at t=10 minutes in 3D control run. a. The plot is an overlay of surface moisture convergence (g kg^{-1} s^{-1}) and wind vectors (m s^{-1}) near the surface. b. The plot is an overlay of perturbation potential temperature (K) and wind vectors (m s^{-1}) near the surface.

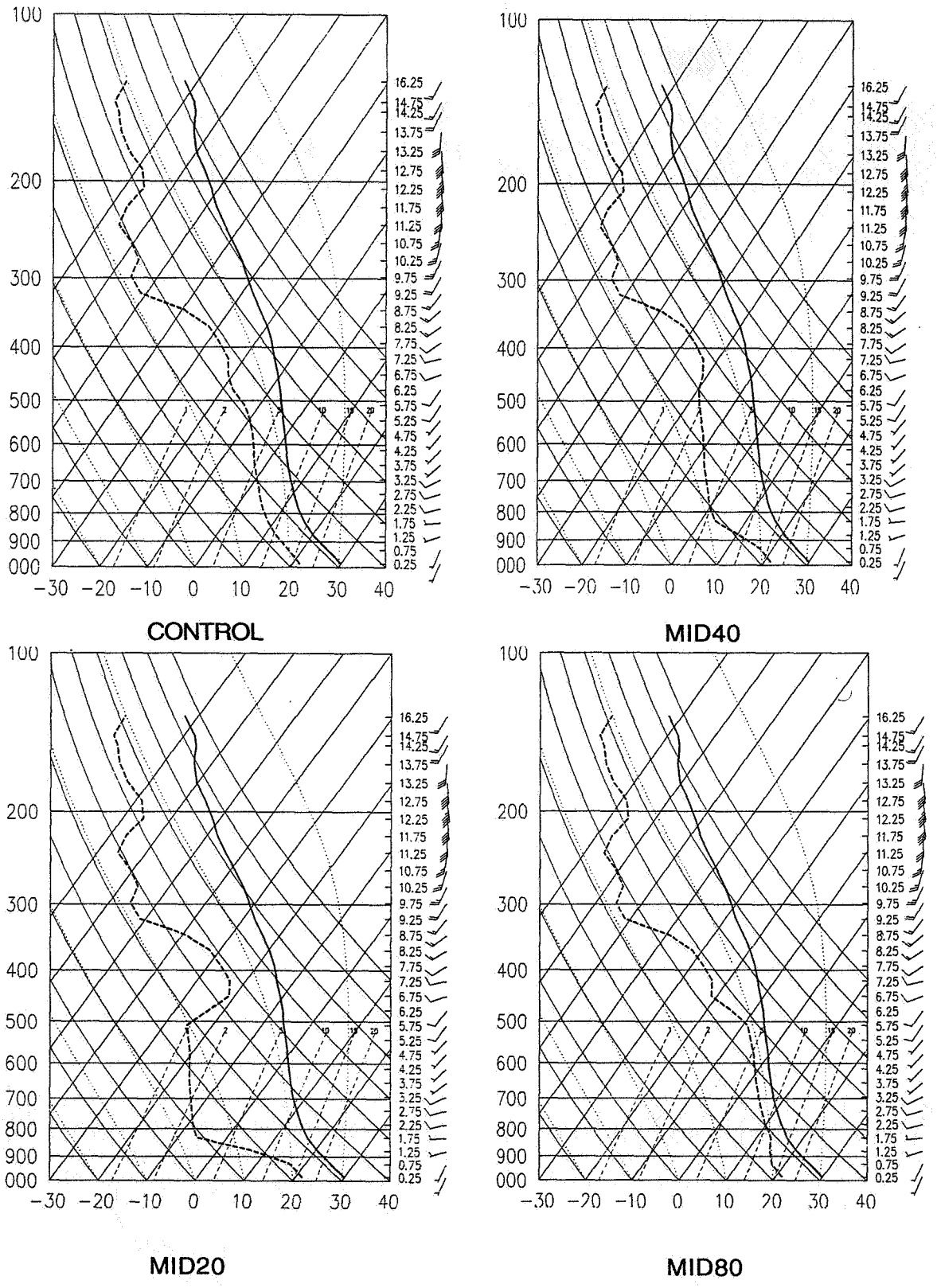

Figure 7-Modified soundings for 2D Mid-Tropospheric experiments.

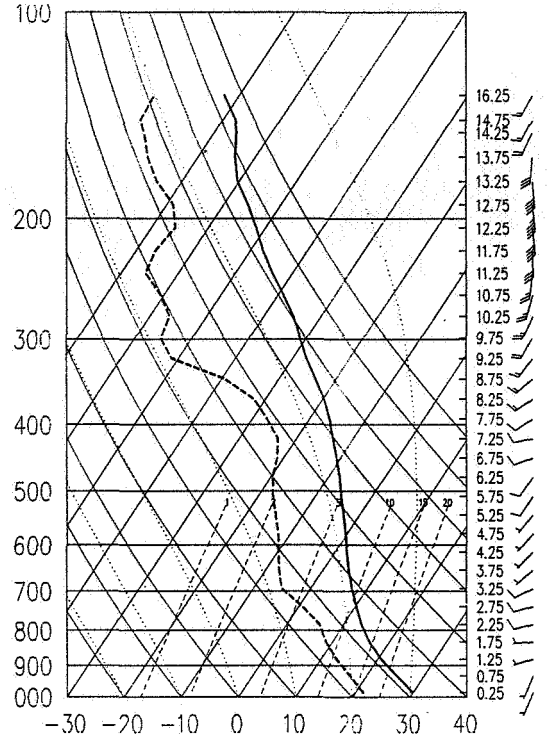

DRY700500

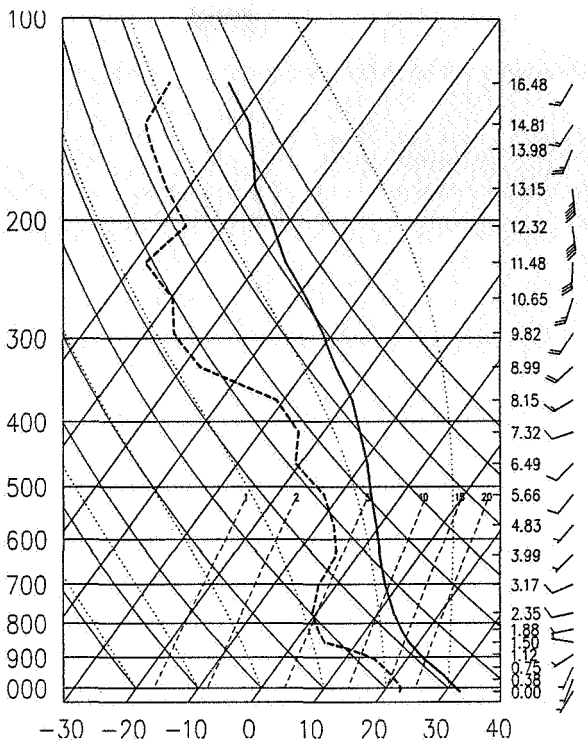

DRY850700

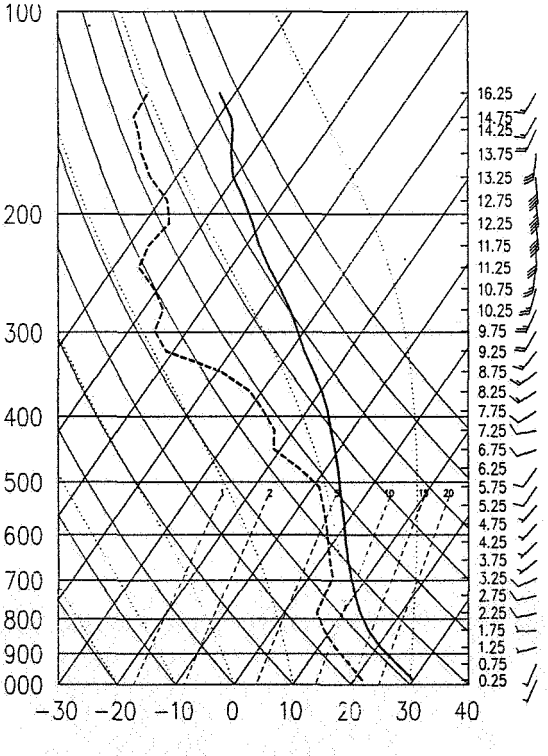

MOIST700500

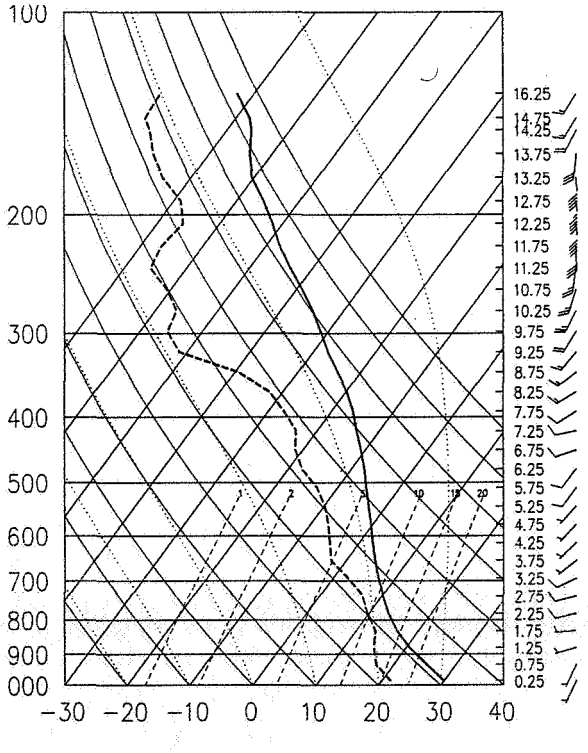

MOIST850700

Figure 7 Continued.

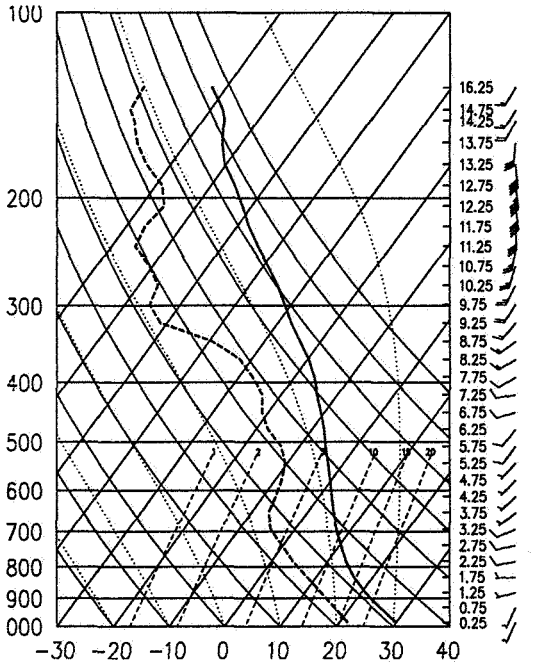

DRYPAR

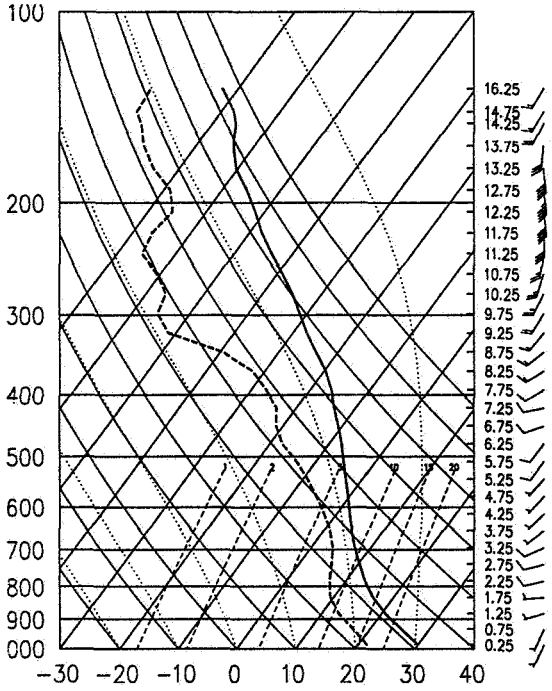

MOISTPAR

Figure 7 Continued.

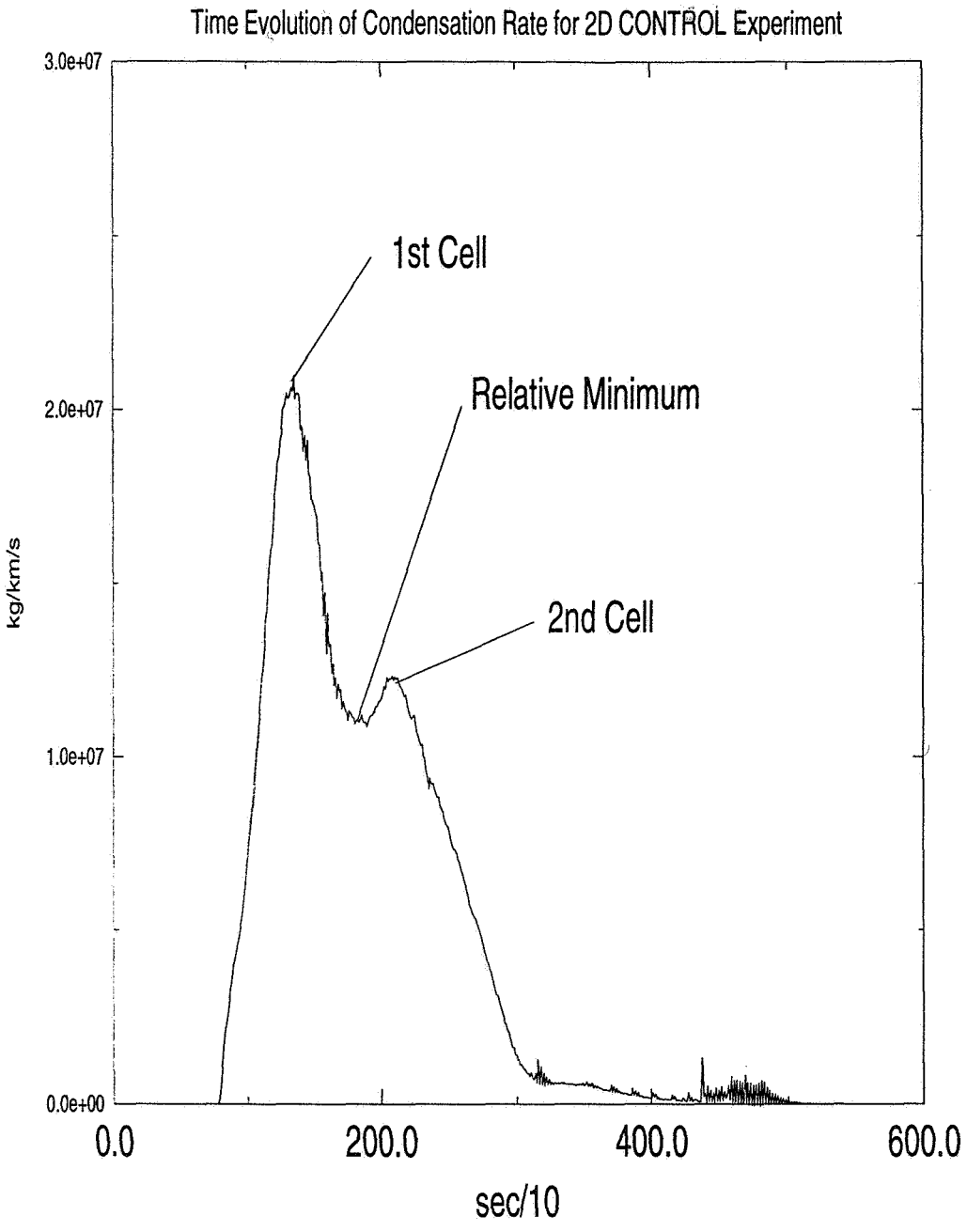

Figure 8-Time series of condensation rate (kg km^{-1} s^{-1}) for 2D **CONTROL** experiment illustrating transition period from exclusively first-cell rainfall to multicellular rainfall.

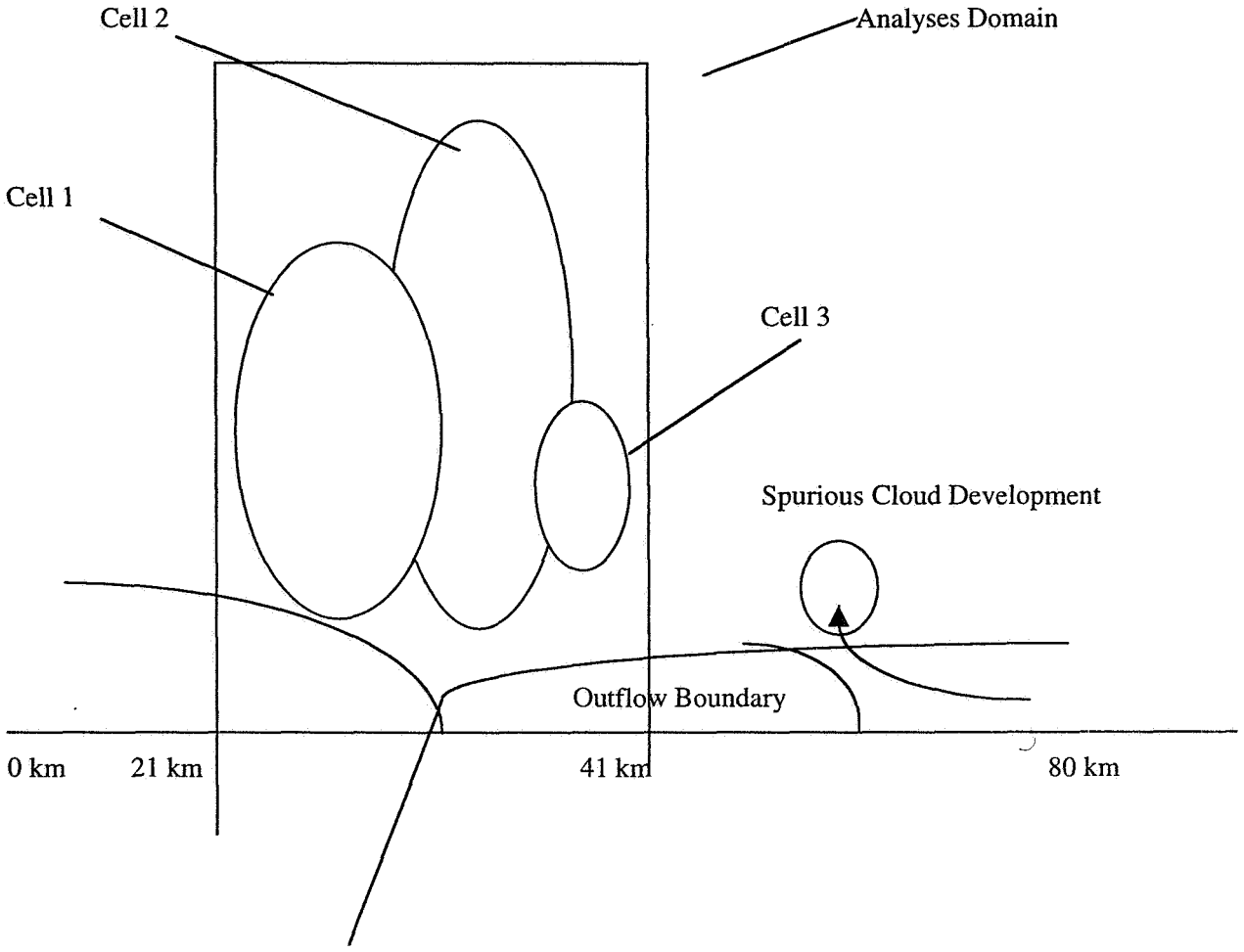

Initial Sea Breeze Front/Outflow Boundary Convergence Point

Figure 9-Conceptualization of the sub-domain used for water budget constituent and rainfall analyses. Cell 1 is the oldest cell (Cell 3 is the youngest cell).

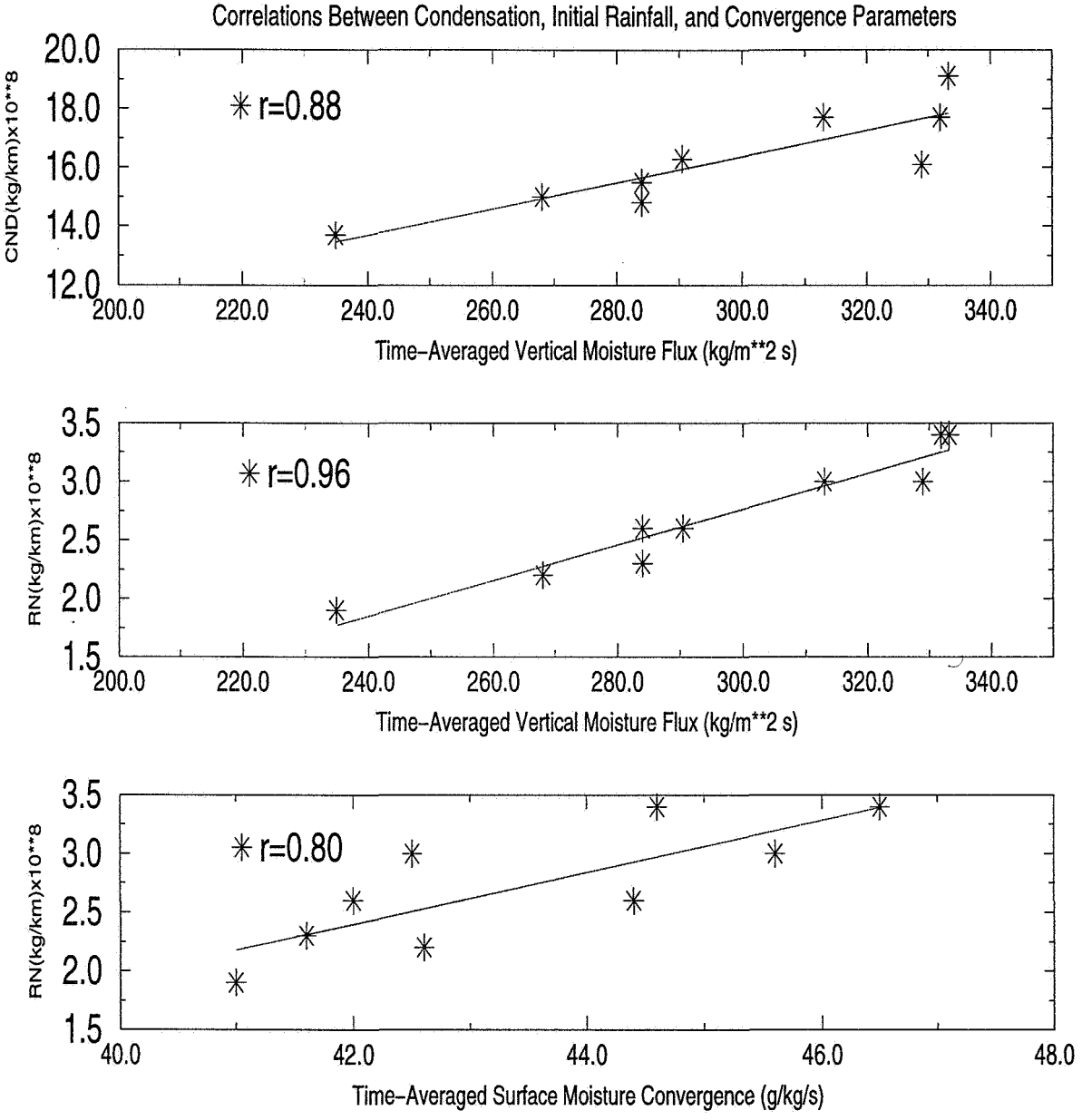

Figure 10-Linear regression analysis of correlations between <VMF>, <SMC>, and total condensation and accumulated rainfall associated with the first convective cell. Top Panel: <VMF>-Condensation. Middle Panel: <VMF>-Rainfall. Bottom Panel: <SMC>-Rainfall.

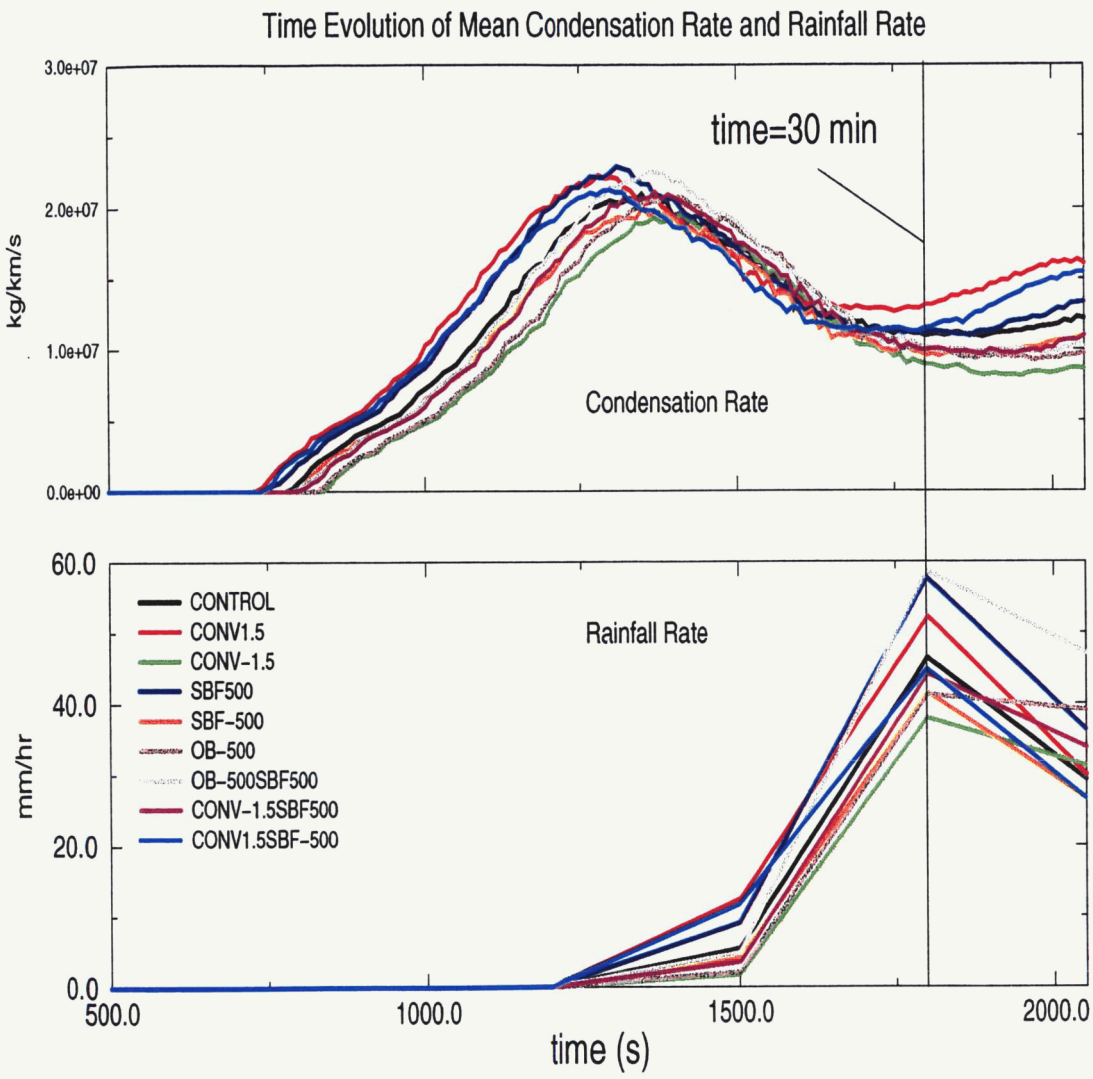

Figure 11-The time series of mean condensation rate (kg km^{-1} s^{-1}) and rainfall rate (mm hr^{-1}) during the first 35 minutes of model run time for each 2D integrated convergence experiment.

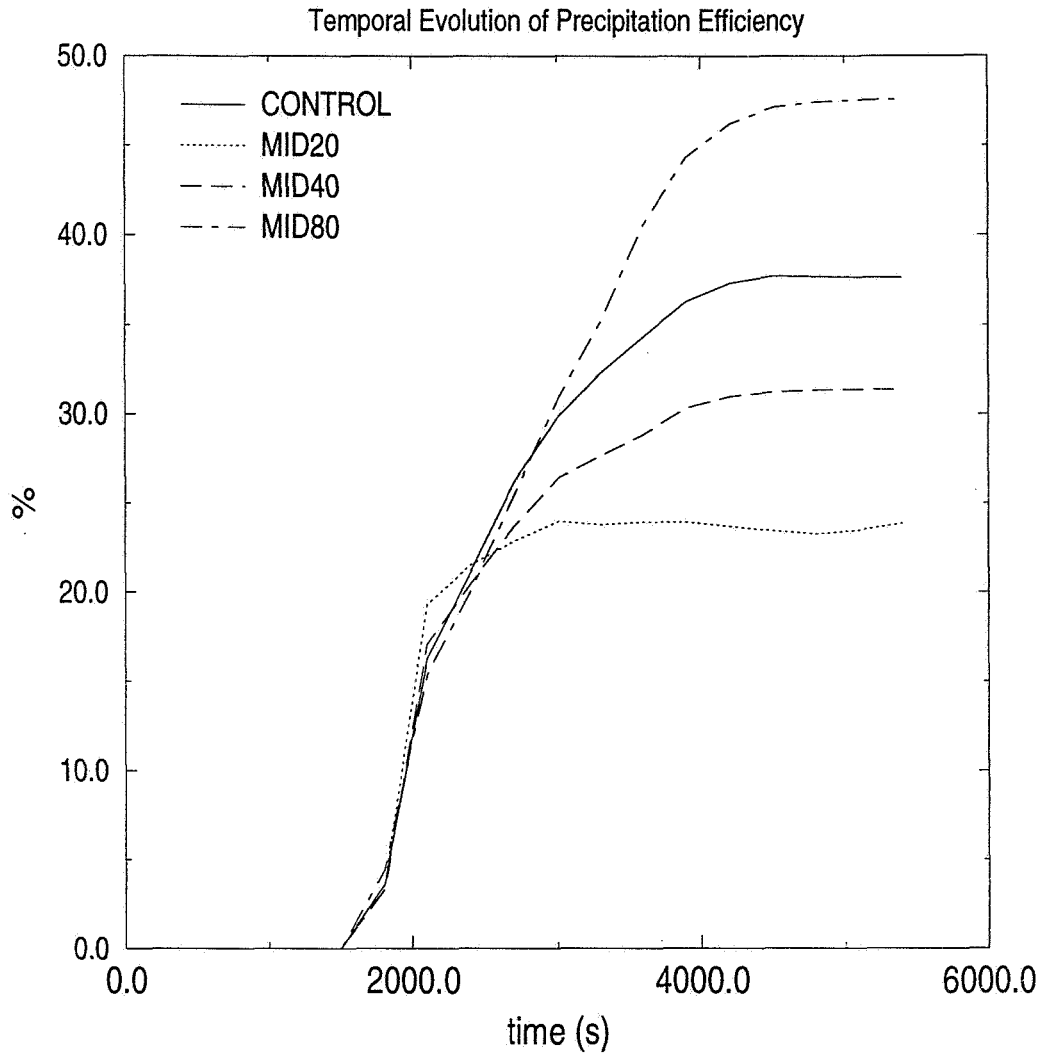

Figure 12-The time evolution of precipitation efficiency (%) in the bulk moisture experiments.

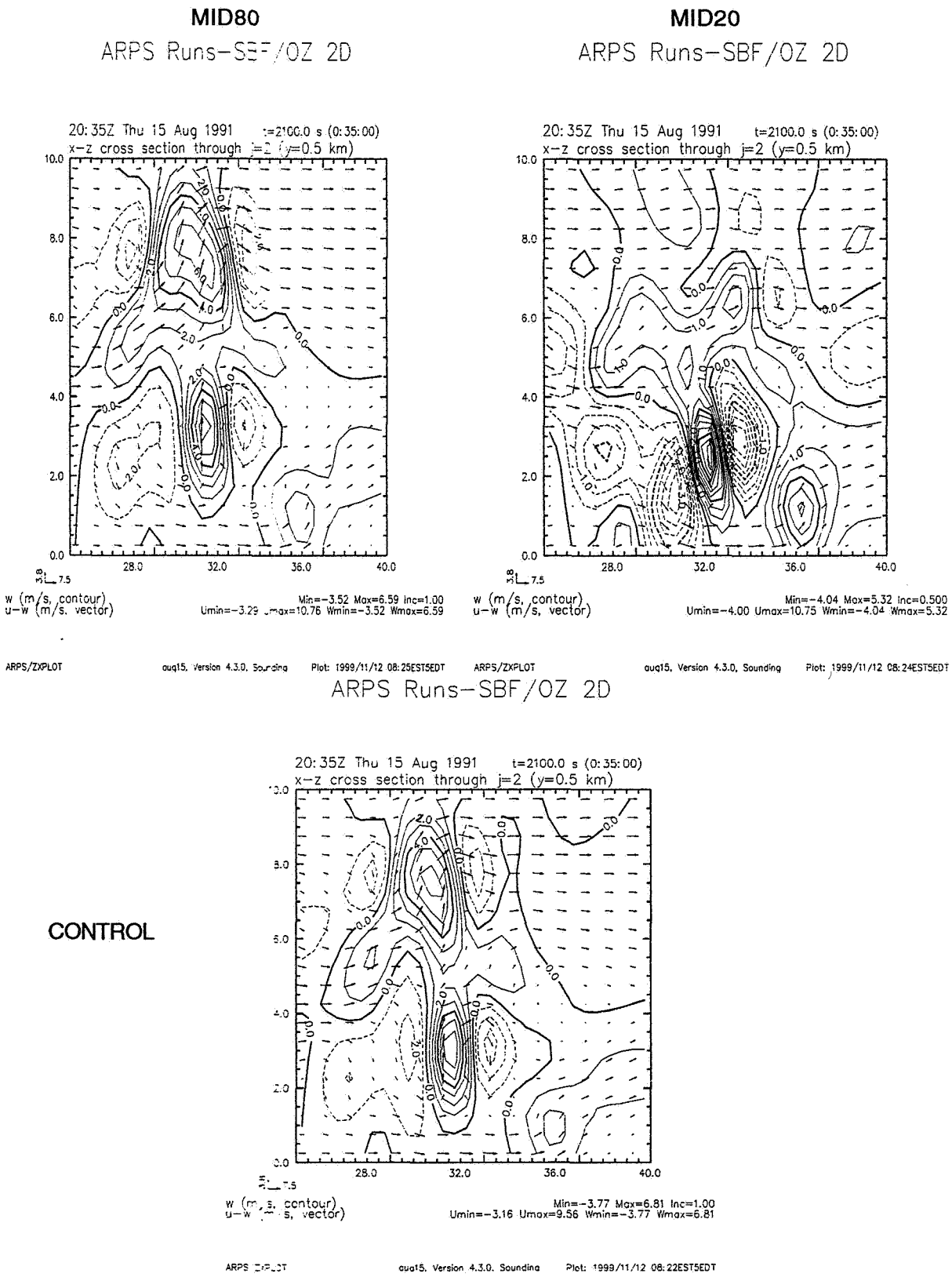

Figure 13-Vertical velocity (m s^{-1}) and wind field (vectors) at t=2100 s for **CONTROL, MID20**, and **MID80.**

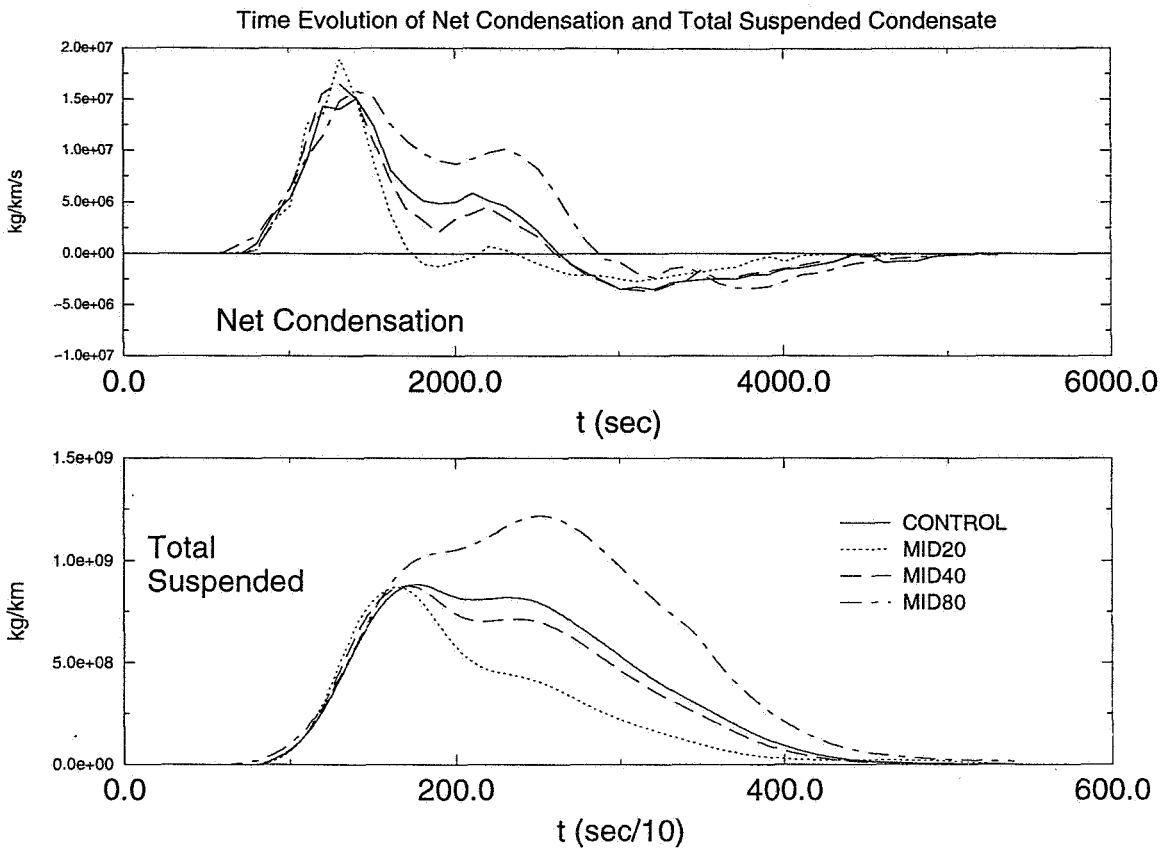

Figure 14-Time series of net condensation (kg km^{-1}) and total suspended condensate (kg km^{-1}) for **CONTROL, MID20, MID40,** and **MID80**.

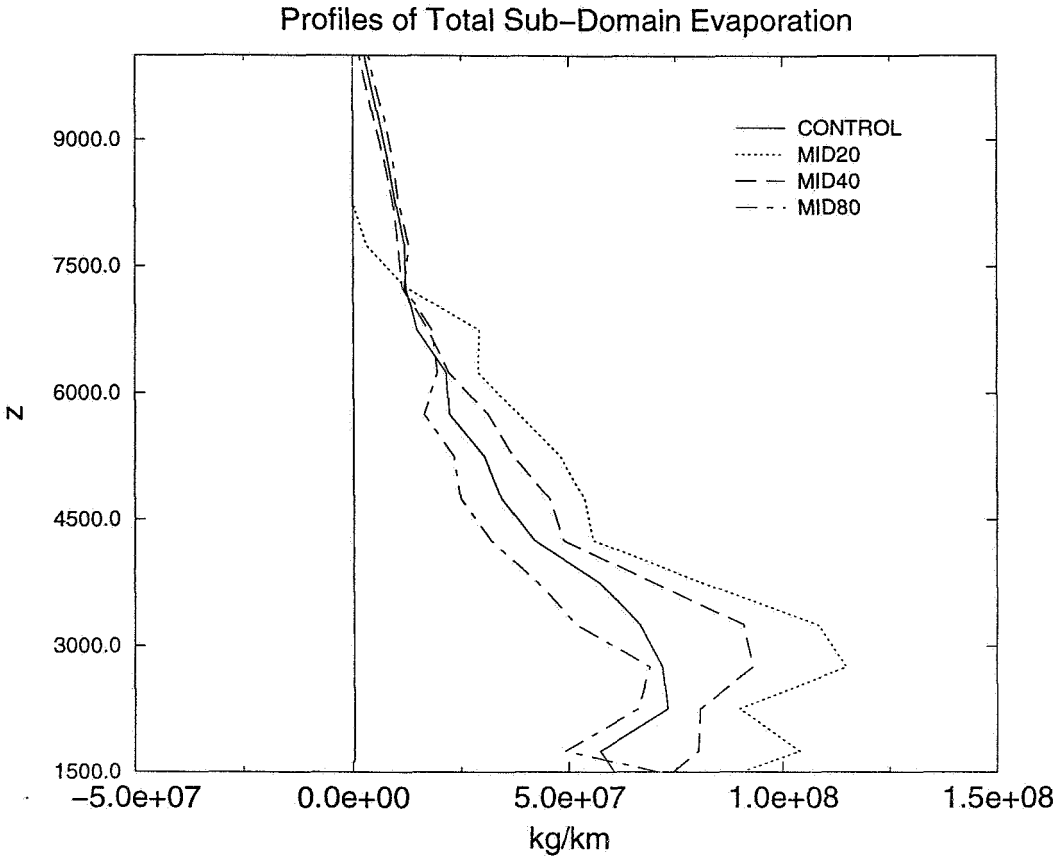

Figure 15-Profiles of total evaporation (kg km^{-1}) from 1.5 km (~850 mb) to 10.0 km in the sub-domain for the bulk moisture experiments. The 500 mb levels is near 5.5 km.

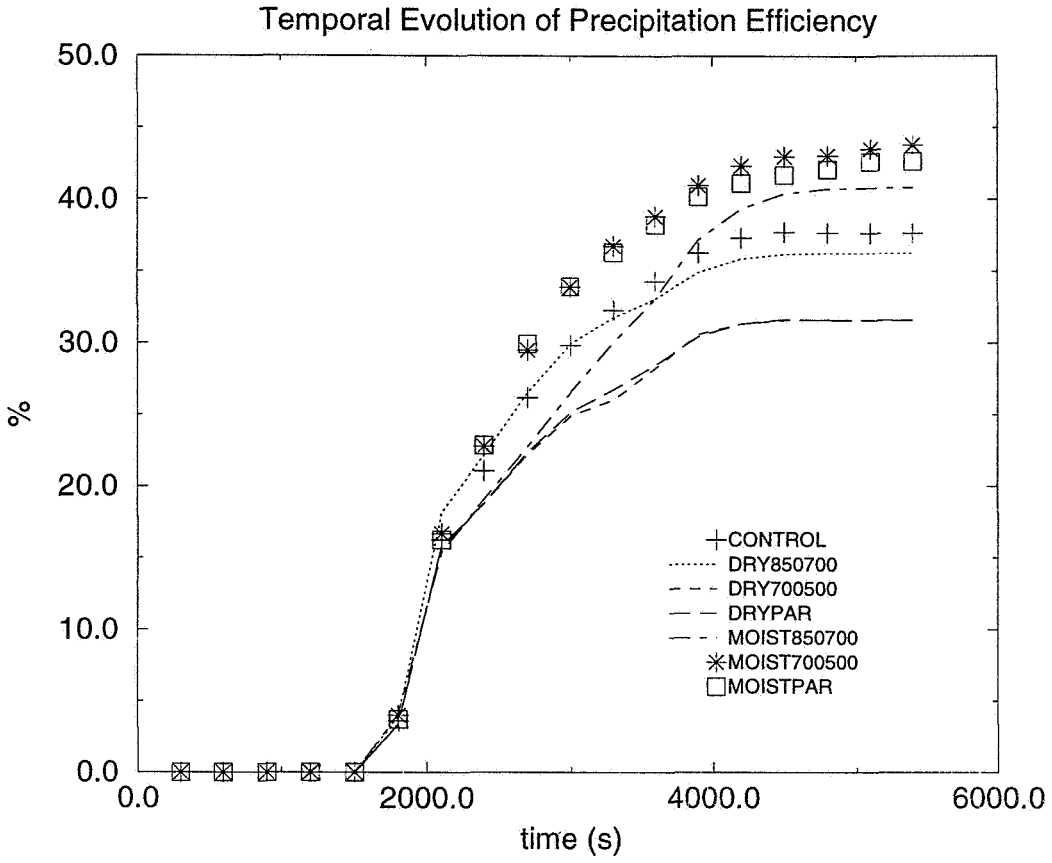

Figure 16-Time series of precipitation efficiency for moisture distribution experiments.

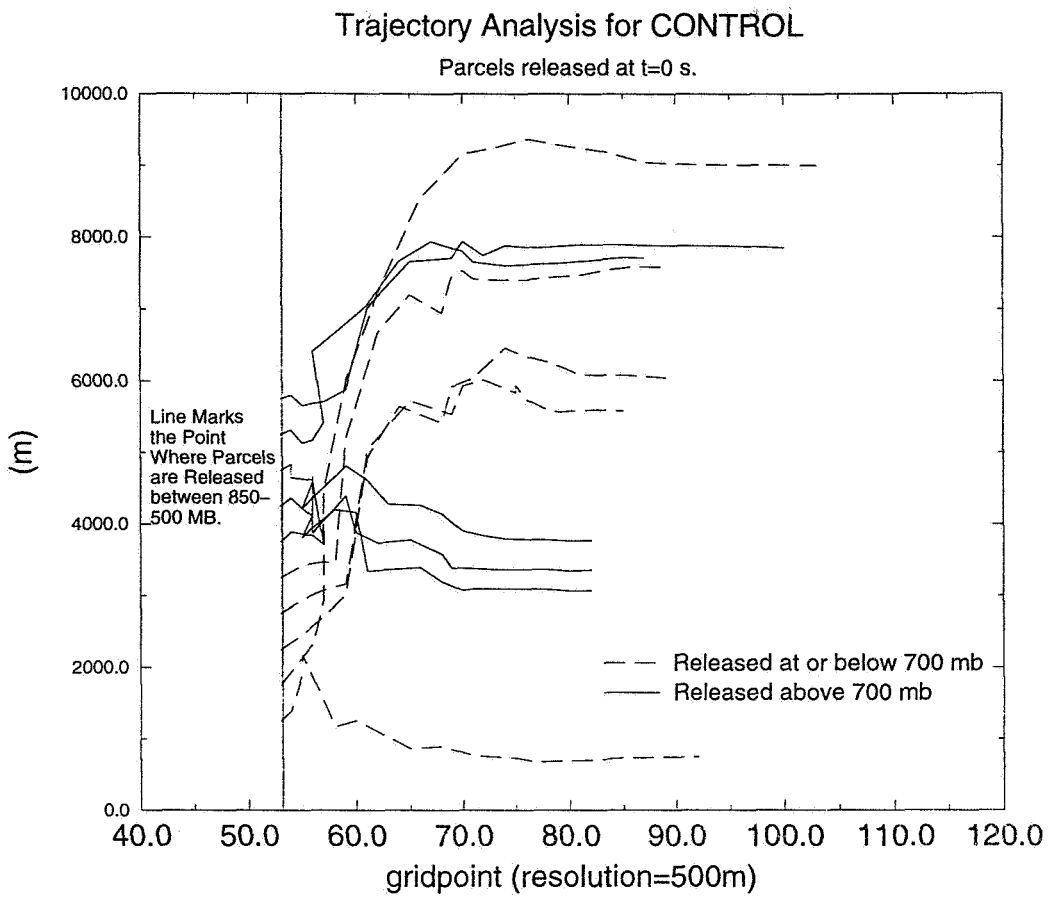

Figure 17-Forward trajectory analysis of the **CONTROL** experiment. Parcels are released at t=0 minutes and traced through t=90.0 minutes.

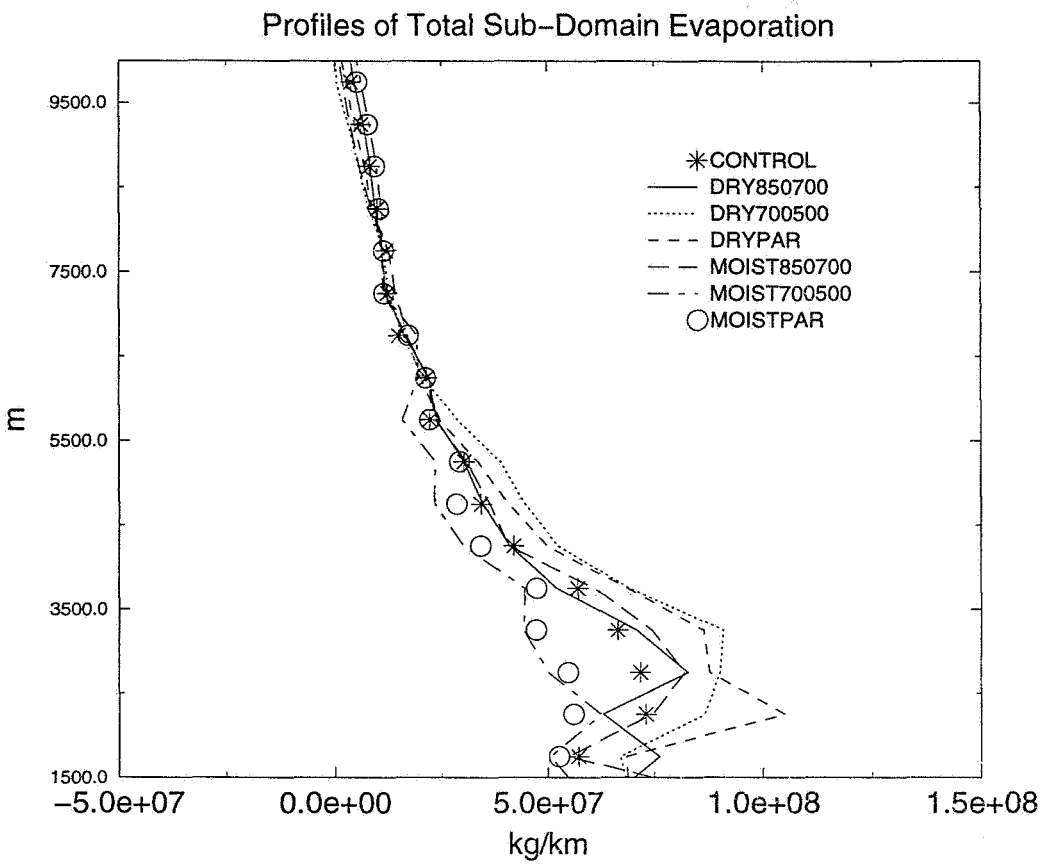

Figure 18-Profiles of total evaporation (kg km^{-1}) from 1.5-10.0 km in the moisture distribution experiments. Note: 850 mb ≅1.5 km, 700 mb ≅ 3.0 km, and 500 mb ≅ 5.5 km.

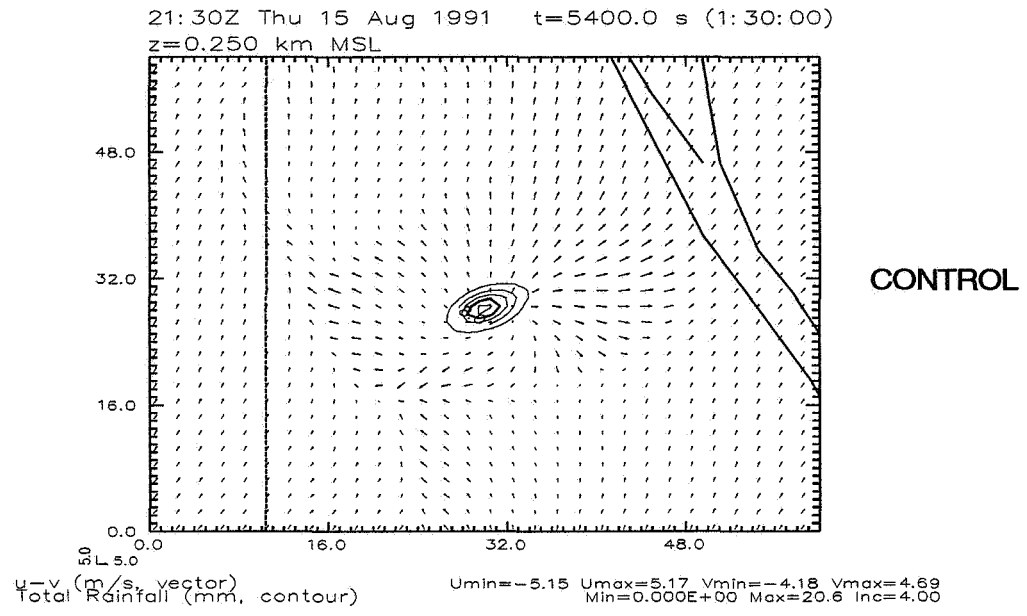

CONTROL

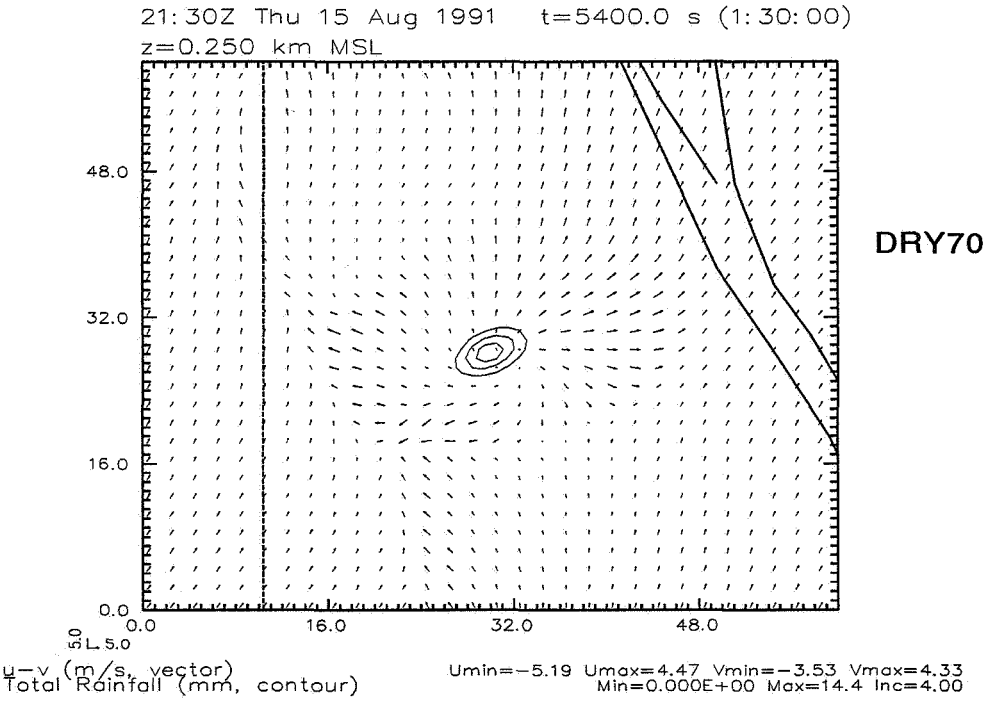

DRY700500

Figure 19-Model-derived total accumulated surface rain at t=90 minutes along with the surface wind field for 3D experiments. Contours are every 4.0 mm.

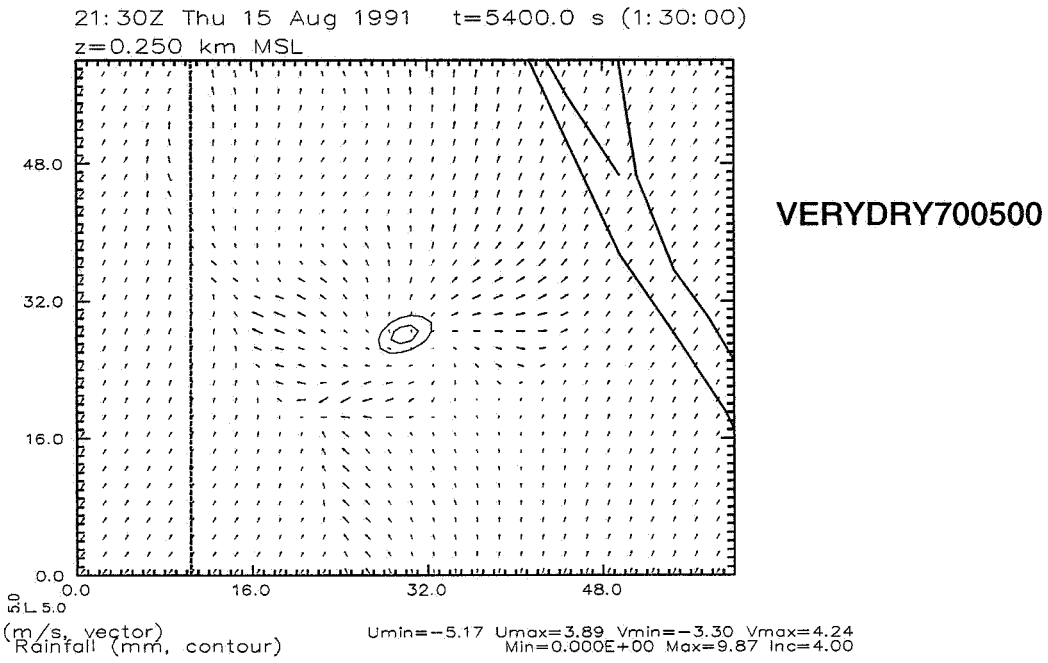

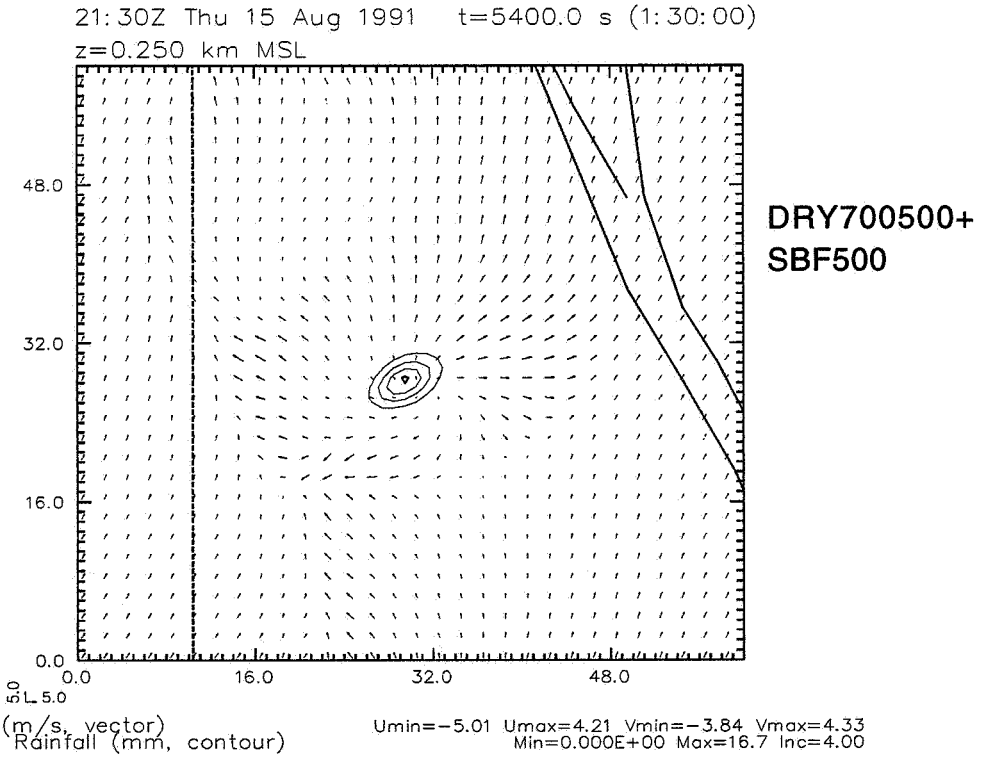

Figure 19 Continued.

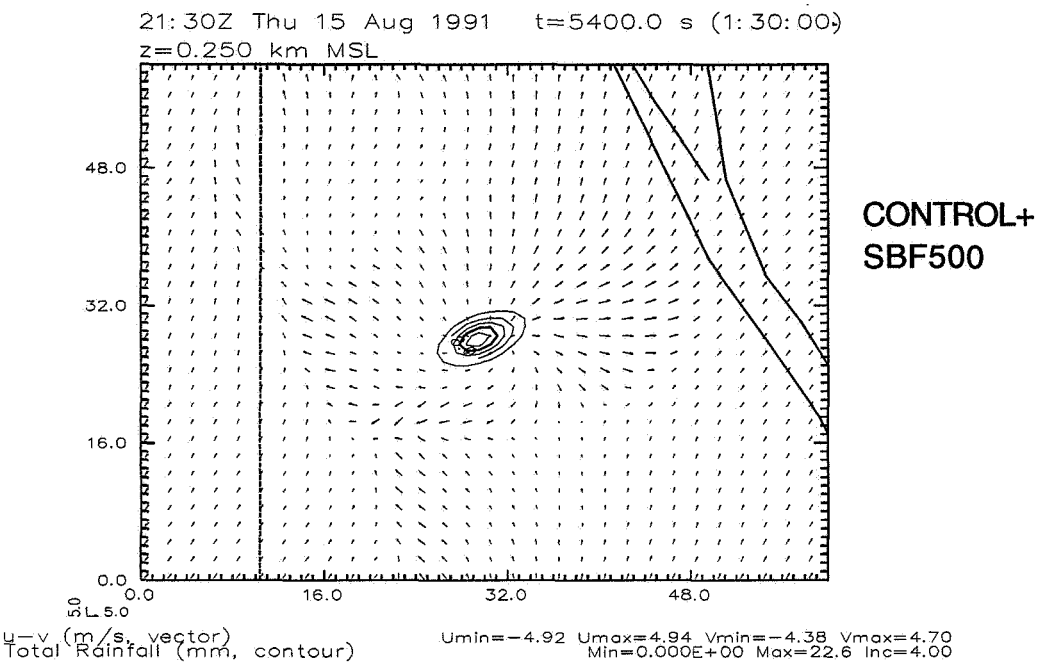

Figure 19 Continued.

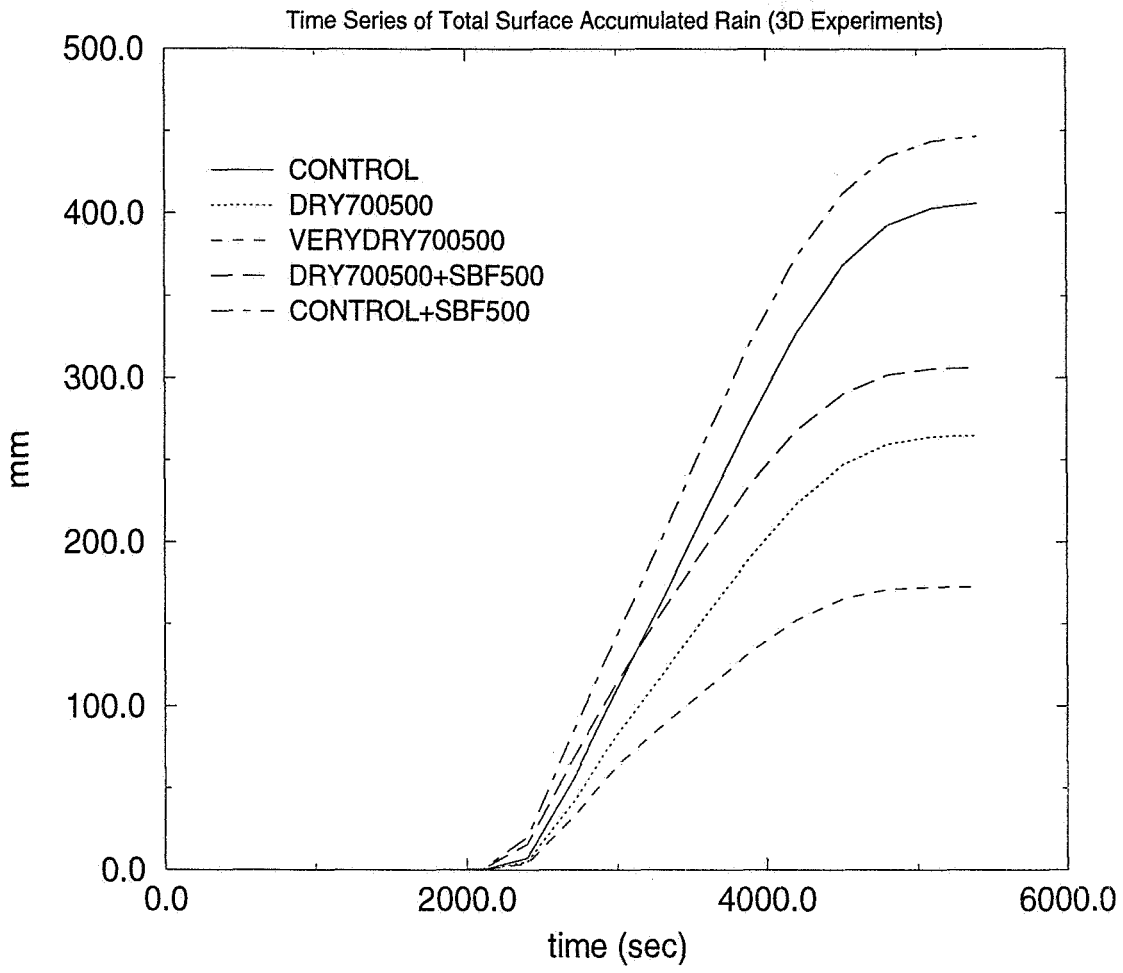

Figure 20-The time series of total accumulated rainfall for the 3D experiments.

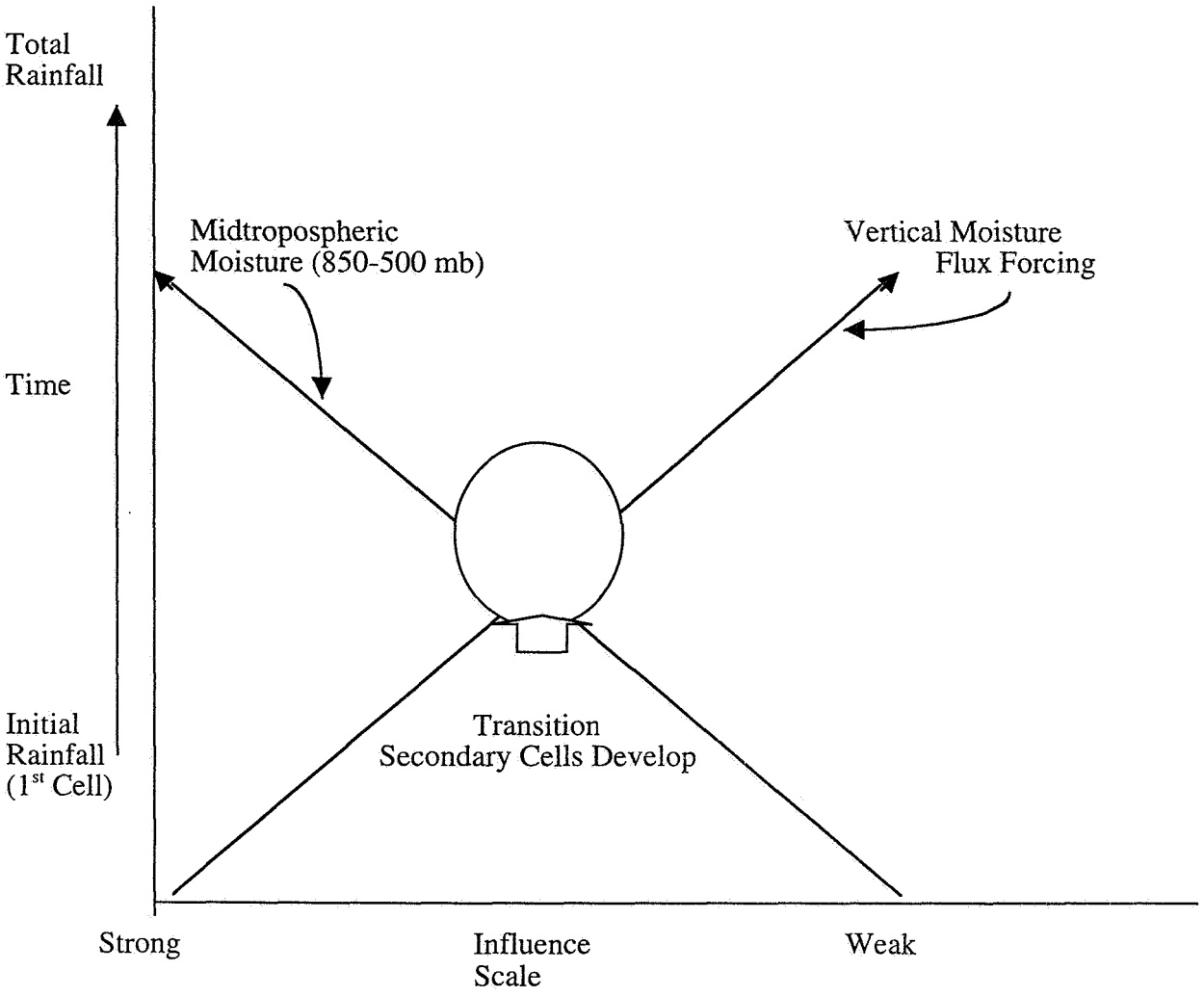

Figure 21-Schematic of the influence of vertical moisture flux and mid-tropospheric moisture on rainfall evolution.

Model Parameter	Description
dx,dy horizontal resolution	500 m (2D), 1.0 km (3D)
dz, vertical resolution	500 m
dtsml, small time step	1 sec
dtbig, big time step	10 sec
total model intergration time (2D, 3D)	1.5 hr
lateral boundary conditions	Klemp-Wilhelmson-type radiation
Sub-grid scale mixing	1.5-order TKE mixing closure
Computational mixing	4^{th}-order mixing scheme
Rayleigh damping sponge	12-17 km
Microphysics	3-Class Ice with Kessler warm rain microphysics
Initialization	Cold pools (following Crook, 1991)

Table 1-Key model parameters.

Experiment	Description
CONTROL	CONTROL
Magnitude	
CONV1.5	Increase surface layer winds behind SBF and OB by 1.5 m s^{-1} (similar to Lee et al. 1991).
CONV-1.5	Decrease surface layer winds behind SBF and OB by 1.5 m s^{-1} (similar to Lee et al. 1991).
Depth	
SBF-500	Decrease SBF depth by 500 meters.
SBF500	Increase SBF depth by 500 meters.
OB-500	Decrease OB depth by 500 meters.
OB-500SBF500	Decrease OB depth by 500 meters, increase SBF by 500 meters.
Magnitude and Depth	
CONV-1.5SBF500	Decrease surface layer winds by 1.5 m s^{-1}, increase SBF depth by 500 meters.
CONV1.5SBF-500	Increase surface layer winds by 1.5 m s^{-1}, decrease SBF depth by 500 meters

Table 2-Description of the 2D Integrated Convergence experiments.

Experiment	Description
CONTROL	CONTROL
Bulk	
MID20	Decrease 850-500 mb relative humidity to 20 percent.
MID40	Decrease 850-500 mb relative humidity to 40 percent.
MID80	Increase 850-500 mb relative humidity to 80 percent.
Distribution	
MOIST700500	Increase 700-500 mb relative humidity to 80 percent.
MOIST850700	Increase 850-700 mb relative humidity to 80 percent.
MOISTPAR	Increase 850-500 mb relative humidity as a parabolic function peaking at 700 mb.
DRY700500	Decrease 700-500 mb relative humidity to 40 percent.
DRY850700	Decrease 850-700 mb relative humidity to 40 percent.
DRYPAR	Decrease 850-500 mb relative humidity as a parabolic function peaking at 700 mb.

Table 3-Description of the 2D Mid-Tropospheric Moisture experiments.

Experiment	Description
CONTROL	60% RH in the 850-500 mb layer.
DRY700500	40% RH at 700-500 mb layer, 60% RH at 850-700 mb
VERYDRY700500	20% RH at 700-500 mb, 60% RH at 850-700 mb
DRY700500+SBF500	Increase SBF depth by 500 m, 40% RH at 700-500 mb
CONTROL+SBF500	Increase SBF depth by 500 m, 60% RH at 700-500 mb

Table 4-Description of Three-Dimensional experiments.

Experiment	<SMC> ($g\ kg^{-1}\ s^{-1}$) $\times 10^3$	<VMF> ($kg\ m^{-2}\ s^{-1}$) $\times 10^3$	CAPE ($J\ kg^{-1}$)	Initial Rainfall ($kg\ km^{-1}$)$\times 10^8$	Initial Condensation ($kg\ km^{-1}$)$\times 10^8$
CONTROL	44.4	290.5	1843	2.6	16.3
Magnitude					
CONV1.5	46.5	333.3	1843	3.4	19.1
CONV-1.5	41.0	235.5	1843	1.9	13.7
Depth					
SBF500	44.6	332.0	1843	3.4	17.7
SBF-500	42.6	268.0	1843	2.2	15.0
OB-500	41.6	284.6	1843	2.3	14.8
OB-500SBF500	42.5	329.3	1843	3.0	16.1
Magnitude and Depth					
CONV-1.5SBF500	42.0	284.6	1843	2.6	15.5
CONV1.5SBF-500	45.6	313.0	1843	3.0	17.7

Table 5-The name of the experiment, the time-averaged, mean surface moisture convergence (<SMC>) at the collision point, the time-averaged, mean vertical moisture flux (VMF) at the collision point, CAPE, total domain accumulated surface rainfall from the first convective cell ($kg\ km^{-1}$), and total domain condensation ($kg\ km^{-1}$) from the first convective cell. Section 4.0 defined initial rainfall.

Experiment	Mean 850-500 mb Precipitable Water (mm)	CAPE ($J\ kg^{-1}$)
CONTROL	18.7	1843
MID20	6.3	1816
MID40	12.5	1830
MID80	25.0	1857

Table 6-A description of the experiment, the mean precipitable water (mm) of the 850-500 mb layer (initial), and the Convective Available Potential Energy (CAPE in J/kg)) of the pre-storm environment for the bulk moisture experiments.

Experiment	C (kg km^{-1})× 10^8	E (kg km^{-1})× 10^8	R (kg km^{-1}) × 10^8	S (kg km^{-1}) × 10^8	PE (%)
CONTROL	23.4	14.5	8.8	.02	37
MID20	21.6	16.4	5.1	.01	23
MID40	23.8	16.3	7.4	.08	31
MID80	31.3	16.2	14.8	.16	47

Table 7-A description of the model results from the bulk moisture experiments in terms of total condensation/deposition (C), total evaporation/sublimation (E), total surface rainfall (R), total suspended condensate, (S) and precipitation efficiency (PE).

Experiment	Mean 850-500 mb Precipitable Water (mm)	CAPE (J kg^{-1})
MOIST700500	22.4	1851
MOIST850700	22.0	1851
MOISTPAR	21.8	1851
DRY700500	15.1	1836
DRY850700	16.0	1836
DRYPAR	14.9	1836

Table 8-A description of the experiment, the mean precipitable water (mm) of the 850-500 mb layer (initial), and the Convective Available Potential Energy (CAPE-J kg^{-1})) of the pre-storm environment for the moisture distribution experiments.

Experiment	C (kg km^{-1})× 10^8	E (kg km^{-1})× 10^8	R (kg km^{-1}) × 10^8	S (kg km^{-1}) × 10^8	PE (%)
CONTROL	23.4	14.5	8.8	.02	37
DRY850700	24.6	15.6	8.9	.03	36
DRY700500	23.2	15.8	7.3	.04	31
DRYPAR	24.5	16.8	7.7	.01	32
MOIST850700	29.6	17.3	12.1	.15	41
MOIST700500	26.6	14.8	11.6	.07	44
MOISTPAR	23.8	13.6	10.1	.04	43

Table 9-A description of the model results from the moisture distribution experiments in terms of total condensation/deposition (C), total evaporation/sublimation (E), total surface rainfall (R), total suspended condensate (S), and precipitation efficiency (PE).

Experiment	1st Cell (mm)	TR (mm)	MAX (mm)	SA(km^2)
DRY700500	5.2	264.8	14.4	28.0
VERYDRY700500	4.0	172.5	9.8	15.0
DRY700500+SBF500	15.7	306.2	16.7	28.0
CONTROL	7.23	406.0	20.6	32.0
CONTROL+SBF500	19.8	446.9	22.6	40.0

Table 10-An overview of the total surface accumulated rainfall in the domain at the end of forty minutes (primarily first cell rainfall), the total surface accumulated rainfall in the domain at t=90 minutes (TR), the maximum surface rainfall (MAX) in the domain, and the approximate surface area covered by rainfall greater than 4.0 mm (SA).